On the Solution of Almansi-Michell's Problem*

Shilei Han† and Olivier A. Bauchau‡
†University of Michigan-Shanghai Jiao Tong University Joint Institute
Shanghai, China
‡The Hong Kong University of Science and Technology
Clear Water Bay, Hong Kong

Abstract

This paper develops a Hamiltonian formalism for the solution of Almansi-Michell's problem that generalizes the corresponding solution of Saint-Venant's problem. Saint-Venant's and Almansi-Michell's problems can be represented as homogenous and non-homogenous Hamiltonian systems, respectively. The solution of Almansi-Michell's problem is determined by the coefficients of the Hamiltonian matrix but also by the distribution pattern of the applied loading. The solution proceeds in two steps: first, for the homogenous problem, a projective transformation is constructed based on a symplectic matrix and second, the effects of the external loading are taken into account by augmenting this projection. With the help of this projection, the three-dimensional governing equations of Almansi-Michell's problem are reduced to a set of one-dimensional beam-like equations, leading to a recursive solution process. Furthermore, the three-dimensional displacement, strain, and stress fields can be recovered from the one-dimensional solution. Numerical examples show that the predictions of the proposed approach are in excellent agreement with exact solutions of two-dimensional elasticity and three-dimensional FEM analysis.

1 Introduction

The "Saint-Venant problem" refers to a three-dimensional beam loaded at its end sections only. Saint-Venant considered prismatic bars made of isotropic materials and whose sectional properties do not vary along their span; he derived exact elasticity solutions for beams under torsion [1] and bending [2]. The "Almansi-Michell problem" refers to a three-dimensional beam loaded by distributed body forces, lateral surface tractions, and forces and moments at its end sections. The problem traces back to Michell and Almansi, who generalized Saint-Venant's problem to more general loading conditions involving uniform lateral tractions [3] and linearly varying surface tractions [4], respectively.

In the classical approach, both Saint-Venant's and Almansi-Michell's problems are solved using the semi-inverse method. For straight bars made of homogenous, isotropic materials, the problem then reduces to the solution of two-dimensional Poisson's equations over the bar's cross-section [5, 6]. The boundary conditions are satisfied exactly at the lateral surface of the beam while those at its end sections are satisfied in a weak sense. The solution is no longer exact near the end sections. Saint-Venant's principle [1, 7], however, implies that the discrepancy between the exact and actual solutions decays away from the end sections rapidly. Consequently, the solutions provided by Saint-Venant, Almansi, and Michell are exact solutions of three-dimensional elasticity "away from the

International Journal of Solids and Structures, **75-76**(1): 156–171, 2015

beam's end sections." Typically, the actual manner in which end loads are applied is unknown, and hence, these exact solutions of elasticity provide the best estimates of the stress states in the beam.

With the increasing use of heterogeneous, anisotropic materials, particularly in the aerospace industry, the generalization of Saint-Venant's and Almansi-Michell's problems to those structures has been the subject of continuous research. For straight beams made such materials, Ieşan [8, 9] developed a systematic approach to the solutions of Saint-Venant's and Almansi-Michell's problems. He assumed that the body forces and lateral surface tractions were polynomial functions of the beam's axial coordinate. Furthermore, Ieşan proved that both Saint-Venant's and Almansi-Michell's problems reduce to a set of generalized plane-strain problems over the beam's cross-section. More recently, Ieşan's approach was generalized by Dong *et al.* [10] for Saint-Venant's problem and by Lin and Dong [11] and Liu and Taciroglu [12] for Almansi-Michell's problem with the aid of a semi-finite element or meshfree discretization for the cross-section. Moreover, the decaying solutions associated with beam's end effects were investigated by Lin *et al.* [13] and Bai *et al.* [14].

Berdichevsky [15] proposed the Variational Asymptotic Method (VAM), in which asymptotic analysis is applied to the energy functional. For beams, the ratio of a typical dimension of the cross-section to the beam's length is a small parameter used in the asymptotic expansion. Using this approach, Saint-Venant's problem is reduced to a two-dimensional analysis over the beam's cross-section. A unified beam theory based on VAM, was further refined by Atilgan and Hodges [16] and Hodges [17]. More recently, Yu [18] extended this approach to the analysis of composite beams subjected to distributed loads.

Giavotto *et al.* [19] presented a different solution strategy for Saint-Venant's problem based on a semi-discretization of three-dimensional beams. They identified two types of solutions: the central solutions, which are the solutions of Saint-Venant's problem, and the extremity solutions, which decay exponentially away from the beam's ends. The decay rates of the extremity solutions provide a quantification of Saint-Venant's principle. Borri *et al.* [20] generalized this methodology to naturally curved and twisted beams. As an extension of this approach, Masarati [21] considered externally applied distributed loads expanded in power series, leading to power series solutions of Almansi-Michell's problem.

Mielke [22, 23] found the central manifold of Saint-Venant's problem. He showed that this central manifold is a finite-dimensional manifold spanned by twelve generalized eigenvectors composed of four Jordan chains. Of these twelve generalized eigenvectors, six correspond to the beam's rigid-body modes while the others six are the fundamental deformation modes of the beam (Saint-Venant's solution): extension, torsion, and bending and shearing in two directions.

Zhong [24] developed novel analytical techniques based on the Hamiltonian formalism. A Hamiltonian operator characterizes the stiffness of the structure and its null and purely imaginary eigenvalues give rise to the solution of Saint-Venant's problem. The eigenvalues with a non-vanishing real part give rise to decaying solutions, and the associated characteristic decay length provide a quantification of Saint-Venant's principle. As previously stated by Mielke, Zhong also identified the Jordan chains associated with the eigenvalues of the Hamiltonian operator with a vanishing real part.

Furthermore, Zhong [25] showed that higher-order Jordan chains exist for the problem of beams subjected to lateral surface tractions. The corresponding higher-order generalized eigenvectors are related to the associated deformation modes. Using the Hamiltonian formalism, he found exact elasticity solutions for a planar beam subjected to uniformly and linearly distributed lateral surface tractions. Zhu *et al.* [26] found the higher-order Jordan chains for planar beams subjected to lateral surface tractions expanded in polynomial series and developed a general approach for such problems.

Ladevèze and Simmonds [27] proposed a new approach for the analysis of straight prismatic beams with piecewise constant cross-sections under arbitrary loading. They found that the complete solution can be divided into a long wavelength part, *i.e.,* the solution of Saint-Venant's and Almansi-Michell's problems, and a short wavelength, localized part, *i.e.,* extremity solutions due

to discontinuity of sectional geometry and external loads. The solutions of Saint-Venant's and Almansi-Michell's problems were derived in terms of the sectional stress resultants, sectional displacements and rotations, and differential operators characterizing the cross-section geometry and material characteristics. Ladevèze and Simmonds' approach was expanded by El Fatmi and Zenzri [28, 29] with the aid of a semi-finite element discretization for cross-sections.

Rand and Rovenski [30] presented a novel formulation and solution strategy for straight, anisotropic beams subjected to lateral surface tractions. The solution strategy is based on a recursive scheme: at each level, a coupled-planar problem is formulated and solved based on results of a corresponding boundary value problem at the previous recurrence step. Analytical solution strategies were used to find solutions for the corresponding two-dimensional boundary value problems. Barber [31] found a general solution for the problem of a three-dimensional prismatic bar subjected to arbitrary lateral surface tractions. He assumed that the distribution can be expanded in finite power series of the axial coordinate. The solution is obtained by repeated differentiation of the tractions with respect to the axial coordinates. A set of recursive sub-problems are solved to construct the generalized solution.

Bauchau and Han [32] developed a systematic approach for the solution of Saint-Venant's problem based on the Hamiltonian formalism. The approach proceeds through a set of structure preserving transformations using symplectic matrices and decomposes the solution into its central and extremity components. The structure preserving transformations lead to a set of linear equations for the nodal warping and sectional compliance matrix; the explicit construction of the Jordan form is thereby avoided. The solutions of Saint-Venant's problem are found by projecting the governing equations onto the subspace of the Hamiltonian matrix associated with its eigenvalues presenting vanishing real parts. The same authors [33] further generalized the approach to initially curved beams undergoing large motion but small strains.

Almansi-Michell's and Saint-Venant's problems can be represented by non-homogenous and homogeneous Hamiltonian systems, respectively. The solutions of Almansi-Michell's problem depend on the coefficient of the Hamiltonian matrix but also on the applied loading distribution pattern, as expected. Consequently, the approach proposed in this paper proceeds in two steps: first, for the homogenous problem, a projective transformation is constructed based on a symplectic matrix; second, the effects of the external loading are taken into account by augmenting this projection. With the help of this projection, the three-dimensional governing equations of Almansi-Michell's problem are reduced to a set of one-dimensional beam-like equations, leading to a recursive solution process. Furthermore, the three-dimensional displacement, strain, and stress fields can be recovered from the one-dimensional solution.

This paper is organized as follows: the kinematics and governing equations of Almansi-Michell's problem are presented in sections 2 and 3, respectively. The construction of projective transformation is discussed in section 4 and leads to the reduced, beam-like equations presented in section 5. Illustrative numerical examples are presented in section 6.

2 Kinematics of the problem

Figure 1 depicts a naturally curved and twisted beam of length L, with a cross-section of arbitrary shape and area $\mathcal{A}$. The region occupied by the beam is generated by sliding the cross-section along the reference line of the beam, which is defined by an arbitrary curve in space denoted $\mathcal{C}$. Curvilinear coordinate α_1 defines the intrinsic parameterization of this curve, *i.e.*, it measures length along $\mathcal{C}$. Point $\mathbf{B}$ is located at the intersection of the reference line with the plane of the cross-section. The unit tangent vector to curve $\mathcal{C}$ is

$$\bar{t} = \frac{\partial \underline{r}_B}{\partial \alpha_1}, \tag{1}$$

where $\underline{r}_B$ is the position vector of point **B** with respect to the origin of the reference frame, $\mathcal{F} = [\mathbf{O}, \mathcal{I} = (\bar{\imath}_1, \bar{\imath}_2, \bar{\imath}_3)]$.

In the reference configuration, the cross-section is defined by frame $\mathcal{F}^* = \left[\mathbf{B}, \mathcal{B}^* = (\bar{b}_1, \bar{b}_2, \bar{b}_3)\right]$. The plane of the cross-section is determined by two mutually orthogonal unit vectors, $\bar{b}_2$ and $\bar{b}_3$; in general, the unit tangent vector, $\bar{t}$, to curve $\mathcal{C}$ is not aligned with unit vector $\bar{b}_1$, as illustrated in fig. 1. A set of material coordinates that represent the configuration of the beam naturally is selected as follows: α_1, α_2, and α_3, where the last two coordinates measure length along the directions of unit vectors $\bar{b}_2$ and $\bar{b}_3$, respectively.

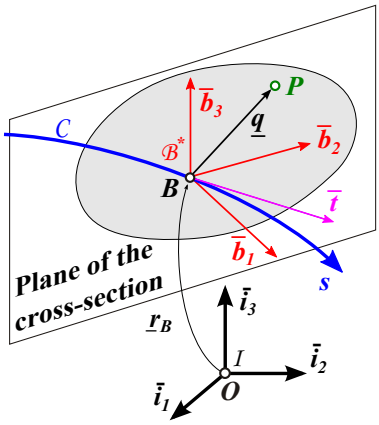

Figure 1: Configuration of a naturally curved and twisted beam.

To balance the orders of magnitude of the stiffness matrices resulting from the formulation, non-dimensional quantities are introduced. The orientation of the sectional plane changes as it slides along curve $\mathcal{C}$. Consequently, basis $\mathcal{B}^*$ is a function of curvilinear variable α_1; the rotation tensor that brings basis $\mathcal{I}$ to $\mathcal{B}^*$ is denoted $\underline{\underline{R}}(\alpha_1)$. The following motion tensor [34] is defined to represent the finite rigid-body motion from frame $\mathcal{F}$ to $\mathcal{F}^*$,

$$\underline{\underline{\mathcal{C}}}(\bar{r}_B, \underline{\underline{R}}) = \begin{bmatrix} \underline{\underline{R}} & \tilde{\bar{r}}_B \underline{\underline{R}} \\ \underline{\underline{0}} & \underline{\underline{R}} \end{bmatrix}. \tag{2}$$

The components of the beam's curvature vector in its initial configuration, resolved in frame $\mathcal{F}^*$, are

$$\tilde{\mathcal{K}}^* = \underline{\underline{\mathcal{C}}}^{-1} \underline{\underline{\mathcal{C}}}', \tag{3}$$

where notation $(\cdot)^*$ indicates tensor components resolved in frame $\mathcal{F}^*$ and $(\cdot)'$ indicates a derivative with respect to α_1. It is verified easily that

$$\tilde{\mathcal{K}}^* = \begin{bmatrix} \tilde{k}^* & \tilde{t}^* \\ \underline{\underline{0}} & \tilde{k}^* \end{bmatrix}, \tag{4}$$

where notation $\widetilde{(\bullet)}$ indicates the skew symmetric matrix constructed from the components of vector $(\bullet)$, and array $\underline{k}^* = \text{axial}(\underline{\underline{R}}^T \underline{\underline{R}}')$ stores the components of the curvature vector associated with rotation field $\underline{\underline{R}}(\alpha_1)$.

2.1 Strain components

With these definitions, the position vector of an arbitrary material point **P** of the beam in its reference configuration becomes

$$\underline{r}(\alpha_1, \alpha_2, \alpha_3) = \underline{r}_B(\alpha_1) + \underline{\underline{R}}(\alpha_1) \underline{q}^*(\alpha_2, \alpha_3), \tag{5}$$

where vector $\underline{q} = \underline{r} - \underline{r}_B$ defines the relative position of point **P** with respect to point **B** and its components resolved in basis $\mathcal{B}^*$ are $\underline{q}^{*T} = \{0, \alpha_2, \alpha_3\}$.

It is now assumed that the beam undergoes small displacements and rotations, and strain components remain very small at all times. After deformation, the position vector of a material point becomes

$$\underline{\underline{R}}(\alpha_1, \alpha_2, \alpha_3) = \underline{r} + \underline{u} = \underline{r} + u_i^* \bar{b}_i, \tag{6}$$

where $\underline{u}$ is the displacement vector and its components resolved in basis $\mathcal{B}^*$ are denoted u_i^*, *i.e.*, $\underline{u} = u_1^* \bar{b}_1 + u_2^* \bar{b}_2 + u_3^* \bar{b}_3$.

The components of the infinitesimal strain tensor are

$$\underline{\gamma}^* = \begin{Bmatrix} \underline{\gamma}^*_O \\ \underline{\gamma}^*_I \end{Bmatrix} = \underline{\underline{A}}\,\underline{u}^{*\prime} + \underline{\underline{B}}\,\underline{u}^*, \tag{7}$$

where the out-of-plane and in-plane strain components are $\underline{\gamma}^*_O = \{\gamma^*_{11}, 2\gamma^*_{12}, 2\gamma^*_{13}\}^T$ and $\underline{\gamma}^*_I = \{\gamma^*_{22}, \gamma^*_{33}, 2\gamma^*_{23}\}^T$, respectively. In eq. (7), the following differential operators were defined

$$\underline{\underline{A}} = \frac{1}{\sqrt{g}} \begin{bmatrix} \underline{\underline{I}} \\ \underline{\underline{0}} \end{bmatrix}, \quad \underline{\underline{B}} = \begin{bmatrix} \underline{\underline{D}}_O \\ \underline{\underline{D}}_I \end{bmatrix}, \tag{8}$$

where scalar $\sqrt{g} = t^*_1 - k^*_3\alpha_2 + k^*_2\alpha_3$ is the determinant of the metric tensor in the reference configuration. In eq. (8), differential operators, $\underline{\underline{D}}_O$ and $\underline{\underline{D}}_I$ were defined as

$$\underline{\underline{D}}_O = \begin{bmatrix} d & -k^*_3 & k^*_2 \\ k^*_3 + \sqrt{g}\dfrac{\partial}{\partial\alpha_2} & d & -k^*_1 \\ -k^*_2 + \sqrt{g}\dfrac{\partial}{\partial\alpha_3} & k^*_1 & d \end{bmatrix}, \; \underline{\underline{D}}_I = \begin{bmatrix} 0 & \sqrt{g}\dfrac{\partial}{\partial\alpha_2} & 0 \\ 0 & 0 & \sqrt{g}\dfrac{\partial}{\partial\alpha_3} \\ 0 & \sqrt{g}\dfrac{\partial}{\partial\alpha_3} & \sqrt{g}\dfrac{\partial}{\partial\alpha_2} \end{bmatrix}, \tag{9}$$

where scalar $d = -(t^*_2 - k^*_1\alpha_3)\partial(\cdot)/\partial\alpha_2 - (t^*_3 + k^*_1\alpha_3)\partial(\cdot)/\partial\alpha_3$. A more detailed derivation of the strain components is given by Han and Bauchau [33].

2.2 Semi-discretization of the displacement field

Beam theory is characterized by one-dimensional, ordinary differential equations governing the displacement field assumed to be a function of the axial variable, α_1, only. In the above paragraphs, the displacement field has been treated as a general vector field depending of three independent variables, α_1, α_2, and α_3. To obtain a one-dimensional formulation, the following semi-discretization of the displacement field is performed,

$$\bar{\underline{u}}^*(\alpha_1, \alpha_2, \alpha_3) = \underline{\underline{N}}(\alpha_2, \alpha_3)\hat{\underline{u}}(\alpha_1), \tag{10}$$

where matrix $\underline{\underline{N}}(\alpha_2, \alpha_3)$ stores the two-dimensional shape functions used in the discretization and array $\hat{\underline{u}}(\alpha_1)$ the nodal values of the non-dimensional displacement field. Notation $\hat{(\cdot)}$ indicates nodal quantities of the discretized variables. This semi-discretization process is shown in fig 2 is a schematic manner: a typical cross-section of the beam is discretized using two-dimensional elements. Let ℓ be the number of nodes used to discretize the beam's cross-section and $n = 3\ell$ the total number of degrees of freedom.

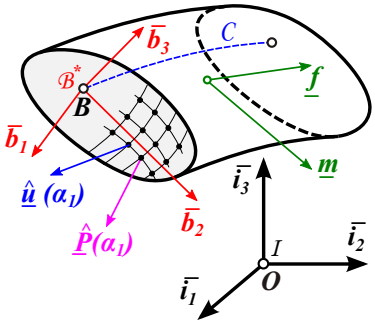

Figure 2: Semi-discretization of the beam.

The same semi-discretization procedure was also adopted by Giavotto *et al.* [19], Borri *et al.* [20], Dong *et al.* [10], and Hodges [17]. Introducing this discretization into eq. (7) yields the components of the strain tensor as

$$\underline{\gamma}^* = \underline{\underline{A}}\,\underline{\underline{N}}\,\hat{\underline{u}}' + \underline{\underline{B}}\,\underline{\underline{N}}\,\hat{\underline{u}}. \tag{11}$$

2.3 Rigid-body motion

For later convenience, an infinitesimal rigid-body motion is introduced $\underline{\mathcal{U}}^T_R = \{\bar{\underline{u}}^T_R, \underline{\phi}^T_R\}$, where $\bar{\underline{u}}_R = \underline{u}_R/a_r$ are the components of a non-dimensional rigid-body translation and $\underline{\phi}_R$ those of a

rigid-body rotation. The components of this rigid-body motion resolved in the material frame are $\underline{\mathcal{U}}_R^* = \underline{\underline{\mathcal{C}}}^{-1}\underline{\mathcal{U}}_R$, where $\underline{\underline{\mathcal{C}}}$ is the motion tensor defined by eq. (2). Because array $\underline{\mathcal{U}}_R$ represents a rigid-body motion, its spatial derivative vanishes, $\underline{\mathcal{U}}_R' = \underline{0}$, and hence, $\underline{\mathcal{U}}_{R,1}^* = -\underline{\underline{\mathcal{C}}}^{-1}\underline{\underline{\mathcal{C}}}_{,1}\underline{\mathcal{U}}_R^* = -\tilde{\mathcal{K}}_1^*\underline{\mathcal{U}}_R^*$, where the second equality results from the definition of generalized curvature tensor in eq. (4).

The infinitesimal rigid-body motion of the beam can be expressed as

$$\begin{Bmatrix} u_1^* \\ u_2^* \\ u_3^* \end{Bmatrix} = \underline{u}_R^* - \tilde{q}^*\underline{\phi}_R^* = \begin{bmatrix} 1 & 0 & 0 & 0 & \alpha_3 & -\alpha_2 \\ 0 & 1 & 0 & -\alpha_3 & 0 & 0 \\ 0 & 0 & 1 & \alpha_2 & 0 & 0 \end{bmatrix} \begin{Bmatrix} \underline{u}_R^* \\ \underline{\phi}_R^* \end{Bmatrix} = \underline{\underline{z}}\,\underline{\mathcal{U}}_R^* = \underline{\underline{N}}\,\underline{\underline{Z}}\,\underline{\mathcal{U}}_R^*, \tag{12}$$

where matrix $\underline{\underline{Z}}$ stacks the rows of matrix $\underline{\underline{z}}$ for each of the nodes of the model. For an infinitesimal rigid-body motion of the beam, the nodal displacements and their axial gradients are found as $\underline{\hat{u}} = \underline{\underline{Z}}\,\underline{\mathcal{U}}_R^*$ and $\underline{\hat{u}}' = -\underline{\underline{Z}}\,\tilde{\mathcal{K}}^*\underline{\mathcal{U}}_R^*$, respectively. Introducing these results into eq. (11) leads to $\underline{\gamma}_R^* = [-\underline{\underline{A}}\,\underline{\underline{N}}\,\underline{\underline{Z}}\,\tilde{\mathcal{K}}^* + \underline{\underline{B}}\,\underline{\underline{N}}\,\underline{\underline{Z}}]\underline{\mathcal{U}}_R^*$ and because the strain field associated with an arbitrary rigid-body motion vanishes, it follows that

$$\underline{\underline{A}}\,\underline{\underline{N}}\,\underline{\underline{Z}}\,\tilde{\mathcal{K}}^* - \underline{\underline{B}}\,\underline{\underline{N}}\,\underline{\underline{Z}} = \underline{\underline{0}}. \tag{13}$$

3 Governing equations

The beam's governing equations will be derived based on Hamilton's formalism. The beam's material constitution is discussed in section 3.1, followed with the introduction of nodal forces and stress resultants in section 3.2. The Lagrangian and Hamiltonian of the system are developed in section 3.3. The virtual work done by the external loads is introduced in section 3.4. Variational principles then yield the non-homogenous Hamiltonian canonical equations of Almansi-Michell's problem.

3.1 Constitutive relations

The beam is assumed to be made of linearly elastic anisotropic materials. The cross-sectional distribution of materials is arbitrary but remains uniform along the beam's span. The Cauchy stress components are denoted as $\underline{\tau}^{*T} = \{\underline{\tau}_O^{*T}, \underline{\tau}_I^{*T}\}$, where $\underline{\tau}_O^{*T} = \{\tau_{11}^*, \tau_{12}^*, \tau_{13}^*\}$ and $\underline{\tau}_I^{*T} = \{\tau_{22}^*, \tau_{33}^*, \tau_{23}^*\}$ stores the out-of-plane and in-plane components, respectively. A linear relationship holds between the components of the Cauchy stress tensor and those of the strain components

$$\underline{\tau}^* = \underline{\underline{\mathcal{D}}}^*\,\underline{\gamma}^*, \tag{14}$$

where the components of the 6×6 material stiffness matrix resolved the material basis are denoted $\underline{\underline{\mathcal{D}}}^*$.

Pre-multiplying eq. (13) by $\underline{\underline{\mathcal{D}}}^*\underline{\underline{A}}\,\underline{\underline{N}}$ and $\underline{\underline{\mathcal{D}}}^*\underline{\underline{B}}\,\underline{\underline{N}}$ and integrating over the beam's cross-section leads to the following matrix identities

$$\underline{\underline{C}}^T\underline{\underline{Z}} = \underline{\underline{M}}\,\underline{\underline{Z}}\,\tilde{\mathcal{K}}^*, \tag{15a}$$

$$\underline{\underline{E}}\,\underline{\underline{Z}} = \underline{\underline{C}}\,\underline{\underline{Z}}\,\tilde{\mathcal{K}}^*, \tag{15b}$$

where non-dimensional matrices $\underline{\underline{M}}$, $\underline{\underline{\bar{C}}}$, and $\underline{\underline{E}}$, of size $n \times n$, are

$$\underline{\underline{M}} = \int_{\mathcal{A}} (\underline{\underline{A}}\,\underline{\underline{N}})^T\underline{\underline{\mathcal{D}}}^*(\underline{\underline{A}}\,\underline{\underline{N}})\,\mathrm{d}\mathcal{A}, \tag{16a}$$

$$\underline{\underline{C}} = \int_{\mathcal{A}} (\underline{\underline{B}}\,\underline{\underline{N}})^T\underline{\underline{\mathcal{D}}}^*(\underline{\underline{A}}\,\underline{\underline{N}})\,\mathrm{d}\mathcal{A}, \tag{16b}$$

$$\underline{\underline{E}} = \int_{\mathcal{A}} (\underline{\underline{B}}\,\underline{\underline{N}})^T\underline{\underline{\mathcal{D}}}^*(\underline{\underline{B}}\,\underline{\underline{N}})\,\mathrm{d}\mathcal{A}. \tag{16c}$$

The non-dimensional differential area is defined as $\mathrm{d}\mathcal{A} = \sqrt{g}\,\mathrm{d}\bar{\alpha}_2\mathrm{d}\bar{\alpha}_3$. Given the distribution of material stiffness properties, these matrices can be evaluated by integration over the cross-section. It is assumed that the curvature vector $\underline{\bar{k}}^*$, material properties $\underline{\underline{\mathcal{D}}}^*$, and cross-sectional shape all remain constant along the beam's span, and hence, matrices $\underline{\underline{M}}$, $\underline{\underline{C}}$, and $\underline{\underline{E}}$ are constant as well.

3.2 Nodal forces and stress resultants

As depicted in fig. 2, stress vectors $\underline{\tau}_O^*$ are acting of the faces of the beam's cross-section. The arrays of non-dimensional nodal forces acting over the cross-section is defined as $\underline{\hat{P}} = \int_{\mathcal{A}} \underline{\underline{N}}^T \underline{\bar{\tau}}_O^*\ \mathrm{d}\mathcal{A}$. Introducing the discretized components of strain tensor given by eq. (13) and material constitutive laws (14) leads to

$$\underline{\hat{P}} = \underline{\underline{M}}\,\underline{\hat{u}}' + \underline{\underline{C}}^T\underline{\hat{u}}. \tag{17}$$

The non-dimensional stress resultants acting on the cross-section, resolved in basis $\mathcal{B}^*$, are $\underline{\bar{\mathcal{F}}}^* = \int_{\mathcal{A}} \underline{\underline{z}}^*\underline{\bar{\tau}}_O^*\ \mathrm{d}\mathcal{A}$. The first three components of array $\underline{\mathcal{F}}^*$ corresponds to the summation of the nodal forces over the beam's cross-section, including the axial force and the two transverse shear forces. The last three components correspond to the sums of the moments of the same forces, including the twisting moment and the two bending moments. Because $\underline{\underline{z}} = \underline{\underline{N}}\,\underline{\underline{Z}}$, the stress resultants can be expressed as

$$\underline{\bar{\mathcal{F}}}^* = \underline{\underline{Z}}^T\underline{\hat{P}}. \tag{18}$$

3.3 Lagrangian and Hamiltonian

The strain energy density of the system, denoted L, is

$$L = \frac{1}{2}\int_{\mathcal{A}} \underline{\gamma}^{*T}\underline{\underline{\mathcal{D}}}^*\underline{\gamma}^*\ \mathrm{d}\mathcal{A}. \tag{19}$$

Introducing the discretized components of strain tensor given by eq. (11), the strain energy density becomes

$$L = \frac{1}{2}\underline{\hat{u}}'\left(\underline{\underline{M}}\,\underline{\hat{u}}' + \underline{\underline{C}}^T\underline{\hat{u}}\right) + \frac{1}{2}\underline{\hat{u}}^T\left(\underline{\underline{C}}\,\underline{\hat{u}}' + \underline{\underline{E}}\,\underline{\hat{u}}\right). \tag{20}$$

For this problem, the strain energy density is also the Lagrangian of the system. Because the nodal forces defined by eq. (17) are $\underline{\hat{P}} = \partial L/\partial\underline{\hat{u}}'$, the nodal forces are the dual variables of Hamilton's formalism. The Hamiltonian of the system, denoted H, is defined via Legendre's transformation [35] as $H = \underline{\hat{P}}^T\underline{\hat{u}}' - L$ and tedious algebra reveals that $H = 1/2\ \underline{\hat{\mathcal{X}}}^T(\underline{\underline{\mathcal{J}}}\,\underline{\underline{\mathcal{H}}})\underline{\hat{\mathcal{X}}}$, where array $\underline{\hat{\mathcal{X}}}$ stores the nodal displacements and forces

$$\underline{\hat{\mathcal{X}}} = \begin{Bmatrix}\underline{\hat{u}}\\ \underline{\hat{P}}\end{Bmatrix}, \tag{21}$$

and matrix $\underline{\underline{\mathcal{H}}}$, of size $2n \times 2n$, is defined as

$$\underline{\underline{\mathcal{H}}} = \begin{bmatrix} -\underline{\underline{M}}^{-1}\underline{\underline{C}}^T & \underline{\underline{M}}^{-1} \\ \underline{\underline{E}} - \underline{\underline{C}}\,\underline{\underline{M}}^{-1}\underline{\underline{C}}^T & \underline{\underline{C}}\,\underline{\underline{M}}^{-1}\end{bmatrix}. \tag{22}$$

Matrix $\underline{\underline{\mathcal{J}}}$ is defined in appendix A and matrix $\underline{\underline{\mathcal{H}}}$ is a constant Hamiltonian matrix, see definition (57).

Identities (15) now imply

$$\underline{\underline{\mathcal{H}}}\,\underline{\underline{\mathcal{Z}}} = -\underline{\underline{\mathcal{Z}}}\,\tilde{\mathcal{K}}^*, \tag{23}$$

where matrix $\underline{\underline{\mathcal{Z}}}$, of size $2n \times 6$, is defined as

$$\underline{\underline{\mathcal{Z}}} = \begin{bmatrix}\underline{\underline{Z}}\\ \underline{\underline{0}}\end{bmatrix} \tag{24}$$

Equation (23) gives the null space of Hamiltonian matrix $\underline{\underline{\mathcal{H}}}$. For a straight beam, the first four columns of generalized curvature $\tilde{\mathcal{K}}^*$ vanish. It follows that the first four columns of $\underline{\underline{\mathcal{Z}}}$ span the null space of Hamiltonian matrix $\underline{\underline{\mathcal{H}}}$ and it can be verified numerically that they span the complete null space of the Hamiltonian. For a curved beam, the null space of matrix $\underline{\underline{\mathcal{H}}}$ is of dimension two and the basis is a combination of the columns of matrix $\underline{\underline{\mathcal{Z}}}$. In summary, the null space of matrix $\underline{\underline{\mathcal{H}}}$ belongs to the space spanned by the columns of matrix $\underline{\underline{\mathcal{Z}}}$. The solvability conditions discussed in section 4.2 rely on this fact.

3.4 External virtual work

The beam is subjected to body forces and lateral surface tractions, generically denoted $\underline{q}^*(\alpha_1, \alpha_2, \alpha_3)$. It is assumed that this loading can be written as

$$\underline{q}^*(\alpha_1, \alpha_2, \alpha_3) = \underline{\underline{P}}(\alpha_2, \alpha_3)\underline{f}(\alpha_1), \tag{25}$$

where matrix $\underline{\underline{P}} = [\underline{P}_1, \cdots, \underline{P}_m]$ and array $\underline{f} = \{f_1, \cdots, f_m\}^T$ store the m loading patterns and the corresponding distribution functions, respectively. Note that the loading patterns vary over the cross-section only whereas the distribution functions depend on the axial variable only.

The virtual work done by the external loads per unit length of the beam is

$$\delta\bar{W}_E = \delta\hat{\underline{u}}^T\hat{\underline{P}}_a = \delta\hat{\underline{u}}^T \begin{cases} [\int_{\mathcal{A}} \underline{\underline{N}}^T\underline{\underline{P}}\ \mathrm{d}\mathcal{A}]\underline{f}, & \text{for body forces;} \\ [\int_{\Gamma} \underline{\underline{N}}^T\underline{\underline{P}}\ \mathrm{d}\Gamma]\underline{f}, & \text{for surface tractions.} \end{cases} \tag{26}$$

Notation $\int_\Gamma(\cdot)\ \mathrm{d}\Gamma$ indicates an integral along the contour, Γ, of the cross-section where the lateral surface tractions are applied. An increment of length along this contour is $\mathrm{d}\Gamma = \|\tilde{g}_1^*\bar{\tau}^*\|\mathrm{d}s$, where s is the curvilinear variable along the contour, $\underline{g}_1^* = \underline{\underline{R}}^T\underline{R}' = \bar{t}^* + \tilde{\bar{k}}^*\bar{q}^*$ the base vector along coordinate line α_1, and $\bar{\tau}^*$ the unit vector tangent to the contour. In eq. (26), the nodal loading array, $\hat{\underline{P}}_a$, can be expressed as $\hat{\underline{P}}_a = \underline{\underline{Q}}\,\underline{f}$, where matrix $\underline{\underline{Q}}$ stores the nodal values of the m loading patterns,

$$\underline{\underline{Q}} = \begin{cases} \int_{\mathcal{A}} \underline{\underline{N}}^T\underline{\underline{P}}\ \mathrm{d}\mathcal{A}, & \text{for body forces;} \\ \int_{\Gamma} \underline{\underline{N}}^T\underline{\underline{P}}\ \mathrm{d}\Gamma, & \text{for surface tractions.} \end{cases} \tag{27}$$

The distribution functions $\underline{f}$ and their k successive derivatives, denoted $\underline{f}^{(i)}$, $i = 1, 2, \cdots, k$, are stored in array $\hat{\underline{f}} = \{\underline{f}, \underline{f}^{(1)}, \cdots, \underline{f}^{(k)}\}^T$. By construction, this array satisfies the following differential equation

$$\hat{\underline{f}}' = \underline{\underline{\mathcal{L}}}\,\hat{\underline{f}}, \tag{28}$$

where matrix $\underline{\underline{\mathcal{L}}}$, of size $m(k+1) \times m(k+1)$, is defined as

$$\underline{\underline{\mathcal{L}}} = \begin{bmatrix} 0 & \underline{\underline{I}} & 0 & \dots & 0 & 0 \\ 0 & 0 & \underline{\underline{I}} & \dots & 0 & 0 \\ \dots & \dots & \dots & \dots & \dots & \dots \\ 0 & 0 & 0 & \dots & 0 & \underline{\underline{I}} \\ 0 & 0 & 0 & \dots & 0 & 0 \end{bmatrix}, \tag{29}$$

and $\underline{\underline{I}}$ denotes the identity matrix of size $m \times m$. Equation (28) implies $\underline{f}^{(k)\prime} = \underline{0}$ and recursive integration leads to the conclusion that $\underline{f}^{(k-i)}$ is an i^{th} order polynomial. Clearly, eq. (28) represents polynomial distribution function up to order k exactly. If the distribution function is not of a polynomial nature, eq. (28) can be viewed as a Taylor series expansion truncated to order k.

3.5 Governing equations

The principle of virtual work, $\int_{\alpha_1}[\delta L - \delta W_E]\ \mathrm{d}\alpha_1 = \int_{\alpha_1}[\delta(\underline{\hat{P}}^T\underline{\hat{u}}' - \bar{L}) - \delta\bar{W}_E]\ \mathrm{d}\alpha_1 = 0$, yields Hamilton's canonical equations, which is composed of two sets of equations. The first set, $\underline{\hat{u}}' = \partial\bar{H}/\partial\underline{\hat{P}}$, is identical to eqs. (17), *i.e.*, defines the nodal forces. The second set, $\underline{\hat{P}}' = -\partial\bar{H}/\partial\underline{\hat{u}} - \underline{\underline{Q}}\,\underline{\hat{f}}$, provides the nodal equilibrium equations. The combination of the two sets results in $2n$ first-order, linear nonhomogeneous ordinary differential equations with constant coefficients

$$\underline{\hat{\mathcal{X}}}' = \underline{\underline{\mathcal{H}}}\,\underline{\hat{\mathcal{X}}} - \begin{bmatrix}\underline{\underline{0}}\\ \underline{\underline{Q}}\end{bmatrix}\underline{f}. \tag{30}$$

The corresponding homogenous problem, $\underline{\mathcal{X}}' = \underline{\underline{\mathcal{H}}}\,\underline{\mathcal{X}}$, provides the governing equations of Saint-Venant's problem.

Clearly, the solution of eq. (30) is determined by the nature of the eigenvalues of Hamiltonian matrix $\underline{\underline{\mathcal{H}}}$, which was discussed by Zhong [25] and Han and Bauchau [32]. For straight beams, the Hamiltonian matrix has null eigenvalues with a multiplicity of twelve; for curved beams, the corresponding matrix has null eigenvalues with a multiplicity of four and a pair of purely imaginary eigenvalues, each of a multiplicity of four. Accordingly, the central solutions are composed of polynomial and trigonometric functions for straight and curved beam problems, respectively. Finally, the eigenvalues of the Hamiltonian matrix presenting non-vanishing real parts give rise to exponentially decaying solutions. Assuming the beam's span to be much larger a characteristic dimension of its cross-section, decaying solutions can be ignored because their effect is significant near the beam's edges only. Consequently, the attention focuses on the solutions associated with the null and purely imaginary eigenvalues of the Hamiltonian. These solutions have been called the "central solutions" by Giavotto *et al.* [19] or "central manifold" by Mielke [23].

To bypass the complexity inherent to the construction of the Jordan chains and associated generalized eigenvectors, projection methods based on symplectic transformations are used. The solutions of Saint-Venant's problem are found by projecting the governing equations onto the subspace of the Hamiltonian matrix associated with its eigenvalues presenting a vanishing real part. For the non-homogenous problem, solutions are expected to depend on these generalized eigenvectors but also on the loading pattern. Consequently, a more general projection is required to solve Almansi-Michell's problem.

4 Projection of the problem

The central solutions of Almansi-Michell's problem will be determined through a projection procedure. Section 4.1 summarizes the projection used by Bauchau and Han [32, 33] for Saint-Venant's problem and this approach is extended to Almansi-Michell's problem in section 4.2.

4.1 Projection of Saint-Venant's problem

The projection procedure can be viewed as a structure preserving coordinate transformation,

$$\underline{\mathcal{X}} = \underline{\underline{\mathcal{S}}}\,\underline{\mathcal{C}}, \tag{31}$$

where matrix $\underline{\underline{\mathcal{S}}}$ is symplectic, see appendix B, and array $\underline{\mathcal{C}}$ stores the reduced set of coordinates,

$$\underline{\underline{\mathcal{S}}} = \begin{bmatrix}\underline{\underline{Z}} & \underline{\underline{W}}\\ \underline{\underline{0}} & \underline{\underline{Y}}\end{bmatrix}, \quad \underline{\mathcal{C}} = \begin{Bmatrix}\underline{\mathcal{U}}^*\\ \underline{\mathcal{F}}^*\end{Bmatrix}. \tag{32}$$

Because matrix $\underline{\underline{\mathcal{S}}}$ is symplectic, see eq. (60), the following identities hold

$$\underline{\underline{Z}}^T\underline{\underline{Y}} = \underline{\underline{I}}, \quad \text{and} \quad \underline{\underline{W}}^T\underline{\underline{Y}} = \underline{\underline{0}}. \tag{33}$$

Pre-multiplying eq. (31) by $\underline{\underline{\mathcal{S}}}^T\underline{\underline{\mathcal{J}}}$ and using property (60) reveals the physical meaning of the reduced coordinates: $\underline{\mathcal{F}}^* = \underline{\underline{Z}}^T\underline{\hat{P}}$ and $\underline{\mathcal{U}}^* = \underline{\underline{Y}}^T\underline{\hat{u}} - \underline{\underline{W}}^T\underline{\hat{P}}$. Array $\underline{\mathcal{F}}^*$, of size 6×1, stores the stress resultants, see eq. (18). Array $\underline{\mathcal{U}}^*$, of size 6×1, stores the average sectional displacements. Matrices $\underline{\underline{W}}$ and $\underline{\underline{Y}}$, both of size $n \times 6$, can now be interpreted as the nodal warping and forces induced by unit sectional stress resultants, respectively.

The governing equations of the homogeneous problem are $\underline{\mathcal{X}}' = \underline{\underline{\mathcal{H}}}\,\underline{\mathcal{X}}$. Introducing coordinate transformation (31) yields $\underline{\underline{\mathcal{S}}}\,\underline{\mathcal{C}}' = \underline{\underline{\mathcal{H}}}\,\underline{\underline{\mathcal{S}}}\,\underline{\mathcal{C}} = \underline{\underline{\mathcal{S}}}\,\underline{\underline{\hat{\mathcal{H}}}}\,\underline{\mathcal{C}}$, where matrix $\underline{\underline{\hat{\mathcal{H}}}}$, of size 12×12, is Hamiltonian because matrix $\underline{\underline{S}}$ is symplectic, see eq. (61). Finally, pre-multiplication by $\underline{\underline{\mathcal{S}}}\,\underline{\underline{\hat{\mathcal{J}}}}$ provides the reduced governing equations as $\underline{\mathcal{C}}' = \underline{\underline{\hat{\mathcal{H}}}}\,\underline{\mathcal{C}}$. In view of identity (23), the upper- and lower-left sub-matrices of $\underline{\underline{\hat{\mathcal{H}}}}$ must be $-\tilde{\mathcal{K}}^*$ and $\underline{\underline{0}}$, respectively, and because it is Hamiltonian, it must present the following structure

$$\underline{\underline{\hat{\mathcal{H}}}} = \begin{bmatrix} -\tilde{\mathcal{K}}^* & \underline{\underline{\mathcal{S}}}^* \\ \underline{\underline{0}} & \tilde{\mathcal{K}}^{*T} \end{bmatrix}, \tag{34}$$

where matrix $\underline{\underline{\mathcal{S}}}^*$ is symmetric and will be interpreted as the beam's sectional compliance matrix.

In summary, the governing equations of the homogenous problem reduce to

$$\underline{\mathcal{U}}^{*\prime} + \tilde{\mathcal{K}}^*\ \underline{\mathcal{U}}^* = \underline{\underline{\mathcal{S}}}^*\underline{\mathcal{F}}^*, \tag{35a}$$

$$\underline{\mathcal{F}}^{*\prime} - \tilde{\mathcal{K}}^{*T}\underline{\mathcal{F}}^* = \underline{0}. \tag{35b}$$

The first six equations defines the beam's sectional constitutive laws: $\underline{\mathcal{E}}^* = \underline{\underline{\mathcal{S}}}^*\underline{\mathcal{F}}^*$, where the sectional strains are defined as

$$\underline{\mathcal{E}}^* = \underline{\mathcal{U}}^{*\prime} + \tilde{\mathcal{K}}^*\underline{\mathcal{U}}^*. \tag{36}$$

The last six equations are the beam equilibrium equations expressed in terms of stress resultants.

4.2 Projection of Almansi-Michell's problem

Almansi-Michell's problem is solved using a projection procedure similar to that summarized in the previous section for Saint-Venant's problem. The coordinate transformation is now

$$\underline{\mathcal{X}} = \underline{\underline{\mathcal{S}}}\,\underline{\mathcal{D}} + \underline{\underline{\mathcal{M}}}\,\underline{\hat{f}}, \tag{37}$$

where symplectic matrix $\underline{\underline{\mathcal{S}}}$ is identical to that defined for the homogeneous problem and the second term of eq. (37) expresses the fact that the solution must depend on the loading and its spanwise derivatives. Matrix $\underline{\underline{\mathcal{M}}}$ and the reduced coordinates have the following form

$$\underline{\underline{\mathcal{M}}} = \begin{bmatrix} \underline{\underline{U}} \\ \underline{\underline{V}} \end{bmatrix} = \begin{bmatrix} \underline{\underline{U}}_0 & \underline{\underline{U}}_1 & \cdots & \underline{\underline{U}}_k \\ \underline{\underline{V}}_0 & \underline{\underline{V}}_1 & \cdots & \underline{\underline{V}}_k \end{bmatrix}, \quad \underline{\mathcal{D}} = \begin{Bmatrix} \underline{\mathcal{U}}^* \\ \underline{\mathcal{P}}^* \end{Bmatrix} \tag{38}$$

where matrices $\underline{\underline{U}}_i$ and $\underline{\underline{V}}_i$, each of size $n \times m$, are yet undetermined and their columns store the warping and nodal forces, respectively, induced by unit values of the i^{th} derivative of distribution function for each of the m loading patterns.

Pre-multiplying eq. (37) by $\underline{\underline{\mathcal{S}}}^T\underline{\underline{\mathcal{J}}}$ and using property (60) reveals the physical meaning of the reduced coordinates

$$\underline{\mathcal{P}}^* = \underline{\mathcal{F}}^* - \underline{\underline{Z}}^T\underline{\underline{V}}\,\underline{\hat{f}}, \tag{39a}$$

$$\underline{\mathcal{U}}^* = \underline{\underline{Y}}^T(\underline{\hat{u}} - \underline{\underline{U}}\,\underline{\hat{f}}) - \underline{\underline{W}}^T(\underline{\hat{P}} - \underline{\underline{V}}\,\underline{\hat{f}}). \tag{39b}$$

Arrays $\underline{\mathcal{P}}^*$ and $\underline{\mathcal{U}}^*$ stores the stress resultants and average sectional displacements; both quantities, however, have been modified by the presence of externally applied loads, as expected.

Introducing coordinate transformation (37) in governing equations (30) yields

$$\left(\underline{\underline{\mathcal{H}}}\,\underline{\underline{\mathcal{M}}} - \underline{\underline{\mathcal{M}}}\,\underline{\underline{\mathcal{L}}} - \begin{bmatrix} \underline{\underline{0}} & \underline{\underline{0}} & \cdots & \underline{\underline{0}} \\ \underline{\underline{Q}} & \underline{\underline{0}} & \cdots & \underline{\underline{0}} \end{bmatrix}\right) \underline{\hat{f}} = \underline{\underline{\mathcal{S}}} \left(\underline{\mathcal{D}}' - \underline{\underline{\hat{\mathcal{H}}}}\,\underline{\mathcal{D}}\right), \tag{40}$$

where matrices $\underline{\underline{\hat{\mathcal{H}}}}$ and $\underline{\underline{\mathcal{L}}}$ are defined by eq. (34) and (29), respectively. Because the problem is linear, the solution is expected to be proportional to the loading, and hence, the right-hand side of eq. (40) should have the following form,

$$\underline{\underline{\mathcal{S}}} \left(\underline{\mathcal{D}}' - \underline{\underline{\hat{\mathcal{H}}}}\,\underline{\mathcal{D}}\right) = \underline{\underline{\mathcal{S}}} \begin{bmatrix} \underline{\underline{\mathcal{R}}} \\ \underline{\underline{\mathcal{T}}} \end{bmatrix} \underline{\hat{f}} = \underline{\underline{\mathcal{S}}} \begin{bmatrix} \underline{\underline{\mathcal{R}}}_0 & \underline{\underline{\mathcal{R}}}_1 & \cdots & \underline{\underline{\mathcal{R}}}_k \\ \underline{\underline{\mathcal{T}}}_0 & \underline{\underline{\mathcal{T}}}_1 & \cdots & \underline{\underline{\mathcal{T}}}_k \end{bmatrix} \underline{\hat{f}}, \tag{41}$$

where unknown matrices $\underline{\underline{\mathcal{R}}}_i$ and $\underline{\underline{\mathcal{T}}}_i$ are of size $6 \times m$. If these matrices can be evaluated, the governing equations reduce to

$$\underline{\mathcal{D}}' - \underline{\underline{\hat{\mathcal{H}}}}\,\underline{\mathcal{D}} = \begin{bmatrix} \underline{\underline{\mathcal{R}}} \\ \underline{\underline{\mathcal{T}}} \end{bmatrix} \underline{\hat{f}}. \tag{42}$$

System (40) can now be recast as a set of recursive equations for the sub-matrices of matrix $\underline{\underline{\mathcal{M}}}$,

$$\underline{\underline{\mathcal{H}}} \begin{bmatrix} \underline{\underline{U}}_0 \\ \underline{\underline{V}}_0 \end{bmatrix} = \begin{bmatrix} \underline{\underline{0}} \\ \underline{\underline{Q}} \end{bmatrix} + \begin{bmatrix} \underline{\underline{Z}} \\ \underline{\underline{0}} \end{bmatrix} \underline{\underline{\mathcal{R}}}_0 + \begin{bmatrix} \underline{\underline{W}} \\ \underline{\underline{Y}} \end{bmatrix} \underline{\underline{\mathcal{T}}}_0, \tag{43a}$$

$$\underline{\underline{\mathcal{H}}} \begin{bmatrix} \underline{\underline{U}}_i \\ \underline{\underline{V}}_i \end{bmatrix} = \begin{bmatrix} \underline{\underline{U}}_{i-1} \\ \underline{\underline{V}}_{i-1} \end{bmatrix} + \begin{bmatrix} \underline{\underline{Z}} \\ \underline{\underline{0}} \end{bmatrix} \underline{\underline{\mathcal{R}}}_i + \begin{bmatrix} \underline{\underline{W}} \\ \underline{\underline{Y}} \end{bmatrix} \underline{\underline{\mathcal{T}}}_i, \quad i = 1, 2, \ldots, k. \tag{43b}$$

Because Hamiltonian matrix $\underline{\underline{\mathcal{H}}}$ is singular, the solvability conditions presented in appendix C must be satisfied for solutions to exist. For simplicity, a slightly more general condition is imposed: the right-hand sides of eqs. (43) should be symplectic orthogonal to matrix $\underline{\underline{\mathcal{Z}}}$ defined by eq. (24). Indeed, as discussed at the end of section 3.3, the null space of $\underline{\underline{\mathcal{H}}}$ belongs to the space spanned by columns of matrix $\underline{\underline{\mathcal{Z}}}$. This solvability condition determines matrices $\underline{\underline{\mathcal{T}}}_i$,

$$\underline{\underline{\mathcal{T}}}_0 = -\underline{\underline{Z}}^T \underline{\underline{Q}}, \tag{44a}$$

$$\underline{\underline{\mathcal{T}}}_i = -\underline{\underline{Z}}^T \underline{\underline{V}}_{i-1}, \quad i = 1, 2, \ldots, k. \tag{44b}$$

The solvability conditions are satisfied for any choice of matrix $\underline{\underline{\mathcal{R}}}$, which is evaluated by setting $\underline{\underline{Y}}^T(\underline{\underline{Z}}\,\underline{\underline{\mathcal{R}}}_0 + \underline{\underline{W}}\,\underline{\underline{\mathcal{T}}}_0) = \underline{\underline{0}}$ and $\underline{\underline{Y}}^T(\underline{\underline{U}}_{i-1} + \underline{\underline{Z}}\,\underline{\underline{\mathcal{R}}}_i + \underline{\underline{W}}\,\underline{\underline{\mathcal{T}}}_i) = \underline{\underline{0}}$, leading to

$$\underline{\underline{\mathcal{R}}}_0 = \underline{\underline{0}}, \tag{45a}$$

$$\underline{\underline{\mathcal{R}}}_i = -\underline{\underline{Y}}^T \underline{\underline{U}}_{i-1}, \quad i = 1, 2, \ldots, k, \tag{45b}$$

where identities (33) were used. Because the solvability conditions are satisfied and eqs. (44) and (45) determine matrices $\underline{\underline{\mathcal{T}}}$ and $\underline{\underline{\mathcal{R}}}$, respectively, systems (43) can be solved recursively to yield matrix $\underline{\underline{\mathcal{M}}}$.

Since the right-hand sides of eqs. (43) are symplectic orthogonal to matrix $\underline{\underline{\mathcal{Z}}}$, the same must hold for the left-hand, *i.e.*, $\underline{\underline{\mathcal{Z}}}^T \underline{\underline{\mathcal{J}}}\,\underline{\underline{\mathcal{H}}}\,\underline{\underline{\mathcal{M}}} = \underline{\underline{0}}$. Using property (57) and identity (23) then yields

$$\tilde{\mathcal{K}}^{*T} \underline{\underline{Z}}^T \underline{\underline{V}} = \underline{\underline{0}}. \tag{46}$$

4.3 Discussion

The proposed approach leads to a set of recursive equations (43) associated with each order of expansion of the distribution functions along the beam's axis. A similar strategy is found in the work of Ieşan [8], Alpdogan *et al.* [36], Rand and Rovenski [30], and Barber [31]. Because these approaches consider straight beams only for which the displacement field is polynomial, recursive solutions of Almansi-Michell's problem are found easily. For curved beam problems, however, the central solution involves trigonometric functions (see Zhong [25] and Han and Bauchau [32] for the planar and spatially curved beams, respectively) and approaches based on polynomial expansions will fail. Recursive equations (43), however, still hold for curved beams because they were derived from the projection procedure.

5 Solution of Almansi-Michell's problem

The reduced governing equations of Almansi-Michell's problem are summarized in section 5.1. The corresponding boundary conditions are derived in section 5.2 and the three-dimensional stress recovery procedure is investigated in section 4.2.

5.1 Reduced governing equations

The governing equations of Almansi-Michell's problem now reduce to system (42)

$$\underline{\mathcal{U}}^{*\prime} + \tilde{\mathcal{K}}^{*}\ \underline{\mathcal{U}}^{*} = \underline{\underline{\mathcal{S}}}^{*}\underline{\mathcal{P}}^{*} + \underline{\underline{\mathcal{R}}}\,\underline{\hat{f}}, \tag{47a}$$

$$\underline{\mathcal{P}}^{*\prime} - \tilde{\mathcal{K}}^{*T}\underline{\mathcal{P}}^{*} = \underline{\underline{\mathcal{T}}}\,\underline{\hat{f}}. \tag{47b}$$

Equations (47a) are the six constitutive laws for the beam. Indeed, introducing the definitions of the sectional strains, eq. (36), and of the reduced coordinates, eq. (39a), yields $\underline{\mathcal{E}}^{*} = \underline{\underline{\mathcal{S}}}^{*}(\underline{\mathcal{F}}^{*} - \underline{\underline{\mathcal{Z}}}^{T}\underline{\underline{\mathcal{V}}}\,\underline{\hat{f}}) + \underline{\underline{\mathcal{R}}}\,\underline{\hat{f}} = \underline{\underline{\mathcal{S}}}^{*}\underline{\mathcal{F}}^{*} + \underline{\underline{\mathcal{B}}}\,\underline{\hat{f}}$, where matrix $\underline{\underline{\mathcal{B}}}$, referred to as the *load influence matrix*, is defined as $\underline{\underline{\mathcal{B}}} = \underline{\underline{\mathcal{R}}} - \underline{\underline{\mathcal{S}}}^{*}\underline{\underline{\mathcal{Z}}}^{T}\underline{\underline{\mathcal{V}}}$. Equations (47b) are the six equilibrium equations of the beam, which can be interpreted by introducing the definition of the reduced coordinates, eq. (39a), leading to $\underline{\mathcal{F}}^{*\prime} - \tilde{\mathcal{K}}^{*T}\underline{\mathcal{F}}^{*} = (\underline{\underline{\mathcal{T}}} + \underline{\underline{\mathcal{Z}}}^{T}\underline{\underline{\mathcal{V}}}\,\underline{\underline{\mathcal{L}}})\underline{\hat{f}}$, where identity (46) was used. Introducing the solvability conditions (44) and definition (29) then yields $\underline{\mathcal{F}}^{*\prime} - \tilde{\mathcal{K}}^{*T}\underline{\mathcal{F}}^{*} = -\underline{\underline{\mathcal{Z}}}^{T}\underline{\underline{Q}}\,\underline{f}$. On the right-hand side of this equation, $\underline{\underline{Q}}\,\underline{f}$ are the externally applied loads and $\underline{\mathcal{A}} = \underline{\underline{\mathcal{Z}}}^{T}\underline{\underline{Q}}\,\underline{f}$ their net resultants.

In summary, the three-dimensional equations of Almansi-Michell's problem, eqs. (30), have been reduced to $12 + m(k+1)$ equations of the following form

$$\underline{\mathcal{E}}^{*} = \underline{\underline{\mathcal{S}}}^{*}\underline{\mathcal{F}}^{*} + \underline{\underline{\mathcal{B}}}\,\underline{\hat{f}}, \tag{48a}$$

$$\underline{\mathcal{F}}^{*\prime} - \tilde{\mathcal{K}}^{*T}\underline{\mathcal{F}}^{*} = -\underline{\mathcal{A}}, \tag{48b}$$

$$\underline{\hat{f}}^{\prime} = \underline{\underline{\mathcal{L}}}\,\underline{\hat{f}}. \tag{48c}$$

Note that the constitutive laws of Saint-Venant's problem, eq. (35a), now become eq. (48a): the externally applied loads affect the beam's constitutive behavior. If the load distribution function is polynomial, *i.e.*, $\underline{f}(\alpha_1) = \sum_{i=0}^{k}\underline{f}^{(i)}(0)\alpha_1^i/i!$, governing equations (48a) and (48b) provide exact solutions of Almansi-Michell's problem [37]

$$\begin{Bmatrix}\underline{\mathcal{U}}^{*}\\ \underline{\mathcal{F}}^{*}\end{Bmatrix}(\alpha_1) = \exp\left(\underline{\underline{\hat{\mathcal{H}}}}\alpha_1\right)\begin{Bmatrix}\underline{\mathcal{U}}_0^{*}\\ \underline{\mathcal{F}}_0^{*}\end{Bmatrix} + \int_0^{\alpha_1}\exp\left[\underline{\underline{\hat{\mathcal{H}}}}(\alpha_1 - u)\right]\begin{Bmatrix}\underline{\underline{\mathcal{B}}}\,\underline{\hat{f}}(u)\\ -\underline{\underline{\mathcal{Z}}}^{T}\underline{\underline{Q}}\,\underline{f}(u)\end{Bmatrix}\mathrm{d}u, \tag{49}$$

where subscript 0 denotes the quantities evaluated at $\alpha_1 = 0$. In eq. (49), the first term is the generalized solution of the homogenous problem, while the second term, a particular solution of the nonhomogenous problem, represents the contribution of distributed loading.

Because the load distribution functions and their partial derivatives are known, only the first twelve equations of system (48) need to be solved. The unknowns are the six rigid-section motion and six stress resultant components. Twelve boundary conditions are needed, six at each end of the beam, as discussed in the next section.

5.2 Boundary conditions

Let $\breve{\underline{u}}$ and $\breve{\underline{P}}$ be the prescribed nodal displacement and forces, respectively, at the end of the beam. To determine the corresponding boundary conditions for Almansi-Michell's problem, the virtual work must vanish: $\delta\hat{\underline{u}}^T(\hat{\underline{P}} - \breve{\underline{P}}) + \delta\hat{\underline{P}}^T(\hat{\underline{u}} - \breve{\underline{u}}) = 0$ at the ends of the beam. This condition is recast in a compact manner as

$$\delta\underline{\mathcal{X}}^T\underline{\underline{\mathcal{J}}}\,(\underline{\mathcal{X}} - \breve{\underline{\mathcal{X}}}) = 0, \tag{50}$$

where $\breve{\underline{\mathcal{X}}}^T = \{\breve{\underline{u}}^T, \breve{\underline{P}}^T\}$. Introducing coordinate transformation (37) and noting that $\delta\underline{\mathcal{X}} = \underline{\underline{\mathcal{S}}}\,\delta\underline{\mathcal{D}}$ yield $\delta\underline{\mathcal{D}}(\underline{\underline{\hat{\mathcal{J}}}}\,\underline{\mathcal{D}} + \underline{\underline{\mathcal{S}}}^T\underline{\underline{\mathcal{J}}}\,\underline{\underline{\mathcal{M}}}\,\underline{\hat{f}} - \underline{\underline{\mathcal{S}}}^T\underline{\underline{\mathcal{J}}}\,\breve{\underline{\mathcal{X}}}) = 0$, leading to

$$\left[\delta\underline{\mathcal{U}}^{*T}, \delta\underline{\mathcal{P}}^{*T}\right]\begin{bmatrix}\underline{\mathcal{P}}^* + \underline{\underline{Z}}^T(\underline{\underline{V}}\,\underline{\hat{f}} - \breve{\underline{P}}) \\ -\underline{\mathcal{U}}^* + \underline{\underline{Y}}^T(\breve{\underline{u}} - \underline{\underline{U}}\,\underline{\hat{f}}) - \underline{\underline{W}}^T(\breve{\underline{P}} - \underline{\underline{V}}\,\underline{\hat{f}})\end{bmatrix} = 0. \tag{51}$$

At a loaded end of the beam, the virtual nodal displacements are arbitrary and the corresponding boundary condition becomes $\underline{\mathcal{P}}^* + \underline{\underline{Z}}^T(\underline{\underline{V}}\,\underline{\hat{f}} - \breve{\underline{P}}) = \underline{0}$. Introducing eq. (39a) then yields $\underline{\mathcal{F}}^* = \underline{\underline{Z}}^T\breve{\underline{P}}$, which implies that the stress resultants must equal the resultant of the externally applied loads, as expected. At a clamped end of the beam, the virtual nodal forces are arbitrary and the corresponding boundary condition becomes $\underline{\mathcal{U}}^* = \underline{\underline{Y}}^T(\breve{\underline{u}} - \underline{\underline{U}}\,\underline{\hat{f}}) - \underline{\underline{W}}^T(\breve{\underline{P}} - \underline{\underline{V}}\,\underline{\hat{f}})$, which can be interpreted as boundary conditions for the average, rigid cross-section motions. In both cases, the boundary conditions are relaxed at the beam's ends, in a manner consistent with Saint-Venant's principle. The average rigid-section motions and stress resultants at the beam's two ends provide twelve conditions to determine the integration constants.

5.3 Three-dimensional stress recovery

Combining eqs. (37) and (39a) yields the nodal displacement and force field

$$\hat{\underline{u}} = \underline{\underline{Z}}\,\underline{\mathcal{U}}^* + \underline{\underline{W}}\,\underline{\mathcal{F}}^* + \underline{\underline{W}}_f\,\underline{\hat{f}}, \tag{52a}$$

$$\hat{\underline{P}} = \qquad \underline{\underline{Y}}\,\underline{\mathcal{F}}^* + \underline{\underline{Y}}_f\,\underline{\hat{f}}, \tag{52b}$$

where $\underline{\underline{W}}_f = \underline{\underline{U}} - \underline{\underline{W}}\,\underline{\underline{Z}}^T\,\underline{\underline{V}}$ and $\underline{\underline{Y}}_f = \underline{\underline{V}} - \underline{\underline{Y}}\,\underline{\underline{Z}}^T\,\underline{\underline{V}}$. The three terms on the right-hand side of eq. (52a) describe the contributions of the rigid-section motion, stress resultants, and external loading, respectively.

In view of eq. (49), if the load distribution function is polynomial, the exact solutions for the nodal displacement and force fields are

$$\begin{aligned}\begin{Bmatrix}\hat{\underline{u}} \\ \hat{\underline{P}}\end{Bmatrix}(\alpha_1) =& \underline{\underline{\mathcal{S}}}\exp(\underline{\underline{\hat{\mathcal{H}}}}\alpha_1)\begin{Bmatrix}\underline{\mathcal{U}}_0^* \\ \underline{\mathcal{F}}_0^*\end{Bmatrix} \\ &+ \underline{\underline{\mathcal{S}}}\int_0^{\alpha_1}\exp\left[\underline{\underline{\hat{\mathcal{H}}}}(\alpha_1 - u)\right]\begin{Bmatrix}\underline{\underline{\mathcal{B}}}\,\underline{\hat{f}}(u) \\ -\underline{\underline{Z}}^T\underline{\underline{Q}}\,\underline{f}(u)\end{Bmatrix}\mathrm{d}u + \begin{bmatrix}\underline{\underline{W}}_f \\ \underline{\underline{Y}}_f\end{bmatrix}\underline{\hat{f}}(\alpha_1),\end{aligned} \tag{53}$$

where the first term is the generalized solution of the homogenous problem and the second and third terms represent the contributions of distributed loads. As evidenced by the last two terms of eq. (53), the effects of the distributed loads are twofold: *(1)* they generate stress resultants and hence, create internal stress and warping, *(2)* they create local stress and warping through the local equilibrium equation directly.

Introducing the nodal displacements and their derivatives into eq. (11) yields the three-dimensional strain field, $\underline{\gamma}^* = \underline{\underline{A}}\,\underline{\underline{N}}(\underline{\underline{Z}}\,\underline{\mathcal{U}}^{*\prime} + \underline{\underline{W}}\,\underline{\mathcal{F}}^{*\prime} + \underline{\underline{W}}_f\,\underline{\hat{f}}^{\prime}) + \underline{\underline{B}}\,\underline{\underline{N}}(\underline{\underline{Z}}\,\underline{\mathcal{U}}^* + \underline{\underline{W}}\,\underline{\mathcal{F}}^* + \underline{\underline{W}}_f\,\underline{\hat{f}})$. This expression can be simplified with the help of eqs. (48) and of identity (13) to find

$$\underline{\gamma}^* = \underline{\underline{A}}\,\underline{\underline{N}}\left[\left(\underline{\underline{Z}}\,\underline{\underline{S}}^* + \underline{\underline{W}}\,\tilde{\mathcal{K}}^{*T}\right)\underline{\mathcal{F}}^* + \underline{\underline{O}}\,\underline{\hat{f}}\right] + \underline{\underline{B}}\,\underline{\underline{N}}\left(\underline{\underline{W}}\,\underline{\mathcal{F}}^* + \underline{\underline{W}}_f\,\underline{\hat{f}}\right), \tag{54}$$

where matrix $\underline{\underline{O}} = \underline{\underline{Z}}\,\underline{\underline{\mathcal{B}}} + \underline{\underline{W}}\,\underline{\underline{\mathcal{T}}} + \underline{\underline{U}}\,\underline{\underline{\mathcal{L}}}$. Equation (54) implies that the three-dimensional strain field at any point of the cross-section can be expressed in terms of the six sectional stress resultants and of the distribution function of the external loads. Finally, the three-dimensional stress field is obtained from the constitutive laws (14) as $\tau^* = \underline{\underline{\mathcal{D}}}^*\underline{\gamma}^*$.

5.4 Summary and discussion

The relationships between the three-dimensional nodal displacements and forces and the beam's one-dimensional rigid cross-section motion and sectional stress resultants are given by eq. (52). A similar equation was also derived by Ladevèze and Simmonds [27] and El Fatmi and Zenzri [28, 29]. Using the notation of Ladevèze and Simmonds, eq. (52) becomes

$$\underline{\hat{u}} = \underline{\hat{I}}\,\underline{u}_R^* + \underline{\hat{\tilde{q}}}^{*T}\underline{\phi}_R^* + \underline{\underline{\mathscr{A}}}\,\underline{N}^* + \underline{\underline{\mathscr{B}}}\;\underline{M}^* + \underline{\underline{W}}_f\underline{\hat{f}}, \tag{55a}$$

$$\underline{\hat{P}} = \qquad\qquad \underline{\underline{\mathscr{A}}}^0\,\underline{N}^* + \underline{\underline{\mathscr{B}}}^0\,\underline{M}^* + \underline{\underline{Y}}_f\underline{\hat{f}}, \tag{55b}$$

where matrices $\underline{\hat{I}}$ and $\underline{\hat{\tilde{q}}}^{*T}$ are the first and last three columns of matrix $\underline{\underline{Z}}$, respectively. The rigid cross-section motion is expressed $\underline{\mathcal{U}}^{*T} = \{\underline{u}_R^{*T}, \underline{\phi}_R^{*T}\}$ and the sectional resultants as $\underline{\mathcal{F}}^{*T} = \{\underline{N}^{*T}, \underline{M}^{*T}\}$. The coefficient matrices $\underline{\underline{\mathscr{A}}}$, $\underline{\underline{\mathscr{B}}}$, $\underline{\underline{\mathscr{A}}}^0$, and $\underline{\underline{\mathscr{B}}}^0$, referred to as "characteristic operators" in refs. [28, 29], are sub-matrices of $\underline{\underline{W}}$ and $\underline{\underline{Y}}$. The symplectic orthogonal conditions (33) correspond to the following properties of the discretized form of the characteristic operators given in refs. [27, 28, 29]: $\underline{\hat{I}}^T\underline{\underline{\mathscr{A}}}^0 = \underline{\underline{I}}$, $\underline{\hat{I}}^T\underline{\underline{\mathscr{B}}}^0 = \underline{\underline{0}}$, $\underline{\underline{\mathscr{A}}}^0 = \underline{\underline{0}}$, $\underline{\hat{\tilde{q}}}^*\underline{\underline{\mathscr{B}}}^0 = \underline{\underline{I}}$, $\underline{\underline{\mathscr{A}}}^{0T}\underline{\underline{\mathscr{A}}} = \underline{\underline{0}}$, $\underline{\underline{\mathscr{A}}}^{0T}\underline{\underline{\mathscr{B}}} = \underline{\underline{0}}$, $\underline{\underline{\mathscr{B}}}^{0T}\underline{\underline{\mathscr{A}}} = \underline{\underline{0}}$, and $\underline{\underline{\mathscr{B}}}^{0T}\underline{\underline{\mathscr{B}}} = \underline{\underline{0}}$. Finally identities $\underline{\underline{Z}}^T\underline{\underline{Y}}_f = \underline{\underline{0}}$ and $\underline{\underline{Z}}^T(\underline{\underline{V}} - \underline{\underline{Y}}\,\underline{\underline{Z}}^T\,\underline{\underline{V}}) = \underline{\underline{0}}$ of the present development are the discretized form of the following properties of the characteristic operators in refs. [27, 28, 29]: $\underline{\underline{\mathscr{A}}}^{0T}\underline{\underline{W}}_f - \underline{\underline{\mathscr{A}}}^T\underline{\underline{Y}}_f = \underline{\underline{0}}$ and $\underline{\underline{\mathscr{B}}}^{0T}\underline{\underline{W}}_f - \underline{\underline{\mathscr{B}}}^T\underline{\underline{Y}}_f = \underline{\underline{0}}$.

For straight beam problems, the proposed approach is identical to that proposed by Ladevèze and Simmonds; indeed, both approaches provide exact solutions of the problem. The approach of Ladevèze and Simmonds proceeds with dual variables (displacement-normal stress pairs) and their "characteristic operators" are the symplectic transformation matrices corresponding to null eigenvalues of the Hamiltonian system. Clearly, they use the Hamiltonian formalism, although the term is not mentioned in their paper.

The Hamiltonian formalism presented here provides a unified analysis procedure for Almansi-Michell's problem. The assumptions made in the derivations above and their implications are summarized as follows. *(1)* Linear elasticity is assumed: strains and warping displacements are small. *(2)* The reference line is of constant curvature along the beam's span. Indeed, the curvature tensor defined by eq. (3) is treated as constant through the developments. *(3)* Although the cross-sectional geometry and material properties are arbitrary, they remain uniform along the beam's span, resulting in a constant Hamiltonian matrix. *(4)* The beam's span is much larger than a

representative dimension of the cross-section. Consequently, the developments focus on the central solution, because the contributions of the extremity solutions are negligible away from the beam ends. This assumption will be further validated by the numerical examples. *(5)* The externally applied body forces and surface tractions can be cast in the form of eq. (25), which implies a separation of variables. The finite number of distribution functions can be interpreted as a truncated Taylor series expansion of the actual distribution.

6 Numerical examples

To validate the proposed approach for the solution of Almansi-Mitchell's problem, a set of numerical examples will be presented. In each case, the following procedure is used: *(1)* determine the beam's sectional stiffness matrix, $\underline{\underline{S}}^*$, and load influence matrix, $\underline{\underline{\mathcal{B}}}^*$, as discussed in section 4.1 and 4.2, respectively; *(2)* solve the governing equations of Almansi-Michell's problem, eqs. (48), with the relaxed boundary conditions on the end sections determined in section 5.2; *(3)* recover the local stress field over the beam's cross-section using eq. (54).

Equation (54) can be recast as

$$\underline{\gamma}^*_{AM} = \underline{\gamma}^*_{SV} + \left[\underline{\underline{A}}\,\underline{\underline{N}}\,\underline{\underline{O}} + \underline{\underline{B}}\,\underline{\underline{N}}\,\underline{\underline{W}}_f\right]\underline{\hat{f}}. \tag{56}$$

The first term describes the strain distribution induced by the stress resultants, $\underline{\mathcal{F}}^*$, and provides the solution of Saint-Venant's problem, denoted $\underline{\gamma}^*_{SV}$. The second term describes the contribution of the distributed loading, $\underline{\hat{f}}$; the sum of the two contributions, denoted $\underline{\gamma}^*_{AM}$, is the solution of Almansi-Michell's problem. When solving beam problems, it is common practice to ignore distributed loading effects: strain distributions are evaluated based on stress resultants only, *i.e.*, the second term of eq. (56) is ignored and $\underline{\gamma}^*_{AM} \approx \underline{\gamma}^*_{SV}$. The rational for this simplification is that the strains induced by stress resultants are assumed to be larger than those induced by the distributed loading. To test the validity of this assumption, the strain distributions $\underline{\gamma}^*_{AM}$ and $\underline{\gamma}^*_{SV}$ will be contrasted in the examples below; the corresponding stress distributions are denoted $\underline{\tau}^*_{AM}$ and $\underline{\tau}^*_{SV}$, respectively.

6.1 Planar rectangular beam

The planar rectangular beam depicted in fig. 3 is subjected to lateral surface tractions, $\underline{p}_t = p_{t1}\bar{b}_1 + p_{t2}\bar{b}_2$ and $\underline{p}_b = p_{b1}\bar{b}_1 + p_{b2}\bar{b}_2$, along its top and bottom edges, respectively. The simply supported beam of length L and height $2h = 0.2L$ is made of homogenous, isotropic material. The following two loading cases are investigated: *(a)* $p_{b1} = q(x_1/L)^2/2$, $p_{t1} = p_{t2} = p_{b2} = 0$, and *(b)* $p_{t2} = -q\sin(x_1/L)$, $p_{t1} = p_{b1} = p_{b2} = 0$.

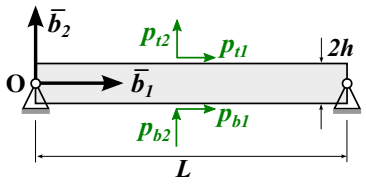

Figure 3: A planar rectangular beam under distributed load.

Six four-node two-dimensional elements were used to mesh the cross-section. A first-order expansion ($k = 1$) was used for the loading distribution function. Timoshenko and Goodier [5] have developed an exact solution of this problem that will be used to calibrate the proposed approach.

Figures 4, 5, and 6 show the distribution of stress components, σ_{11}/q, σ_{22}/q, and σ_{12}/q, respectively, through the beam's thickness at mid-span, for loading case (a). In these figures, the solid line depicts the exact solution [5], while the predictions of the present approach ($\underline{\tau}^*_{AM}$) are indicated with symbols ($\circ$). For reference, the stress distributions predicted by Saint-Venant's solution ($\underline{\tau}^*_{SV}$) are shown with a dashed line.

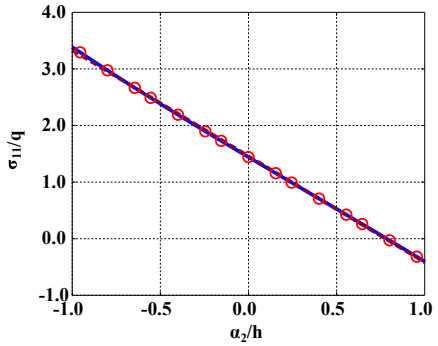

Figure 4: Distribution of stress component σ_{11}/q, case (a).

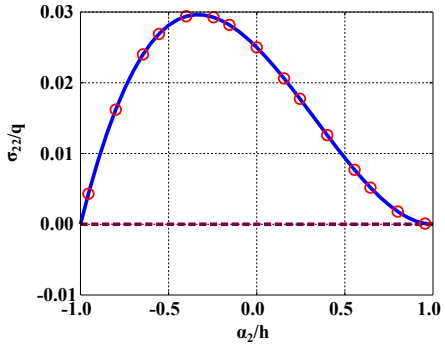

Figure 5: Distribution of stress component σ_{22}/q, case (a).

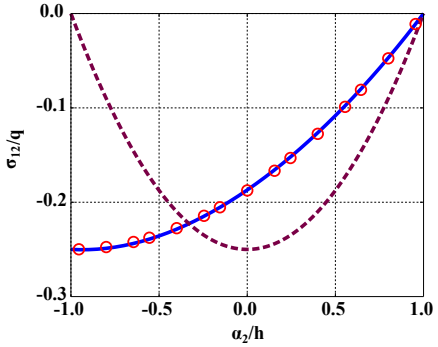

Figure 6: Distribution of stress component σ_{12}/q, case (a).

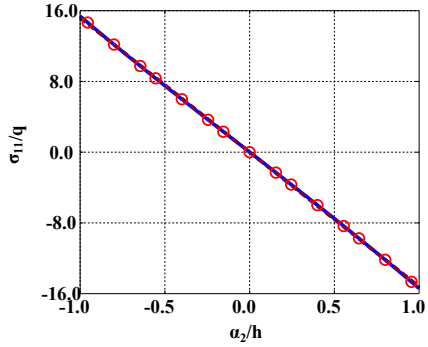

Figure 7: Distribution of stress component σ_{11}/q, case (b).

The predictions of the proposed approach are in excellent agreement with those of the exact solution. While the distributed loading has little effect on the axial stress distribution (fig. 4), significant differences are observed for the transverse (fig. 5) and shear stress (fig. 6) components.

The corresponding results for loading case (b) are shown in figs. 7 and 8. For reasons of symmetry, stress component σ_{12} vanishes at the beam's mid-span and hence, stress gradients, $\partial\sigma_{12}/\partial\alpha_1$, were evaluated instead, as depicted in fig. 9. The predictions of the proposed approach are in excellent agreement with those of the analytical solution.

6.2 Planar curved beam

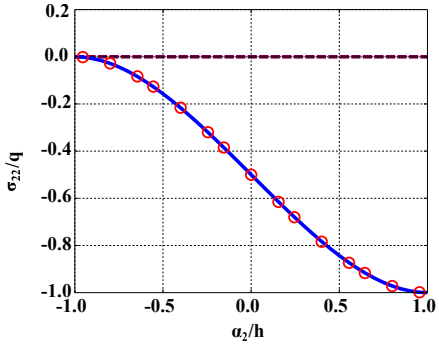

Figure 8: Distribution of stress component σ_{22}/q, case (b).

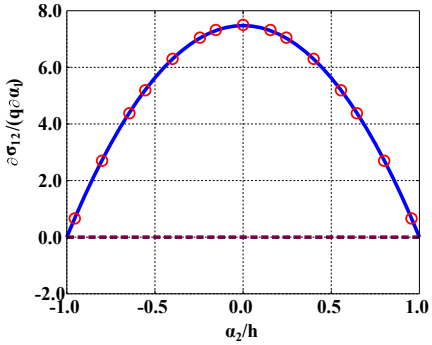

Figure 9: Distribution of stress component gradient $\partial\sigma_{12}/(q\partial\alpha_1)$, case (b).

The planar circular beam depicted in fig. 10 is cantilevered at one end and subjected to lateral surface tractions $\underline{p}_o = p_{o1}\bar{b}_1 + p_{o2}\bar{b}_2$ and $\underline{p}_i = p_{i1}\bar{b}_1 + p_{i2}\bar{b}_2$ along its outer and inner edges, respectively. The beam is made of homogenous, isotropic material, has a radius $R = 1$ m, a thickness $2h = 0.2$ m, and spans an angle of $\pi/3$ rad. At its other end, the beam is subject to three stress resultants: an axial force, N_T, a shear force, Q_T, and a bending moment, M_T, with the positive directions shown in fig. 10. The following two loading cases are investigated: *(a)* $p_{o2} = -\cos(2\pi x_1/L)$ N/m, $N_T =$ - 0.0314286 N, $M_T = 0.0314286$ N·m ($Q_T = p_{o1} = p_{i1} = p_{i2} = 0$), and *(b)* $p_{i1} = -\sin(2\pi x_1/L)$ N/m, $N_T =$ - 0.154286 N, $M_T = 0.0192857$ N·m, ($Q_T = p_{o1} = p_{o2} = p_{i2} = 0$).

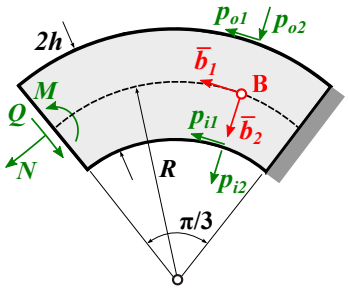

Figure 10: A planar circular beam under distributed loading.

An exact solution of the problem is provided by Ding *et al.* [38]. For the proposed approach, six four-node two-dimensional elements were used to mesh the cross-section. Stress component distributions through the beam's thickness resolved in material basis $\mathcal{B}^*$ were evaluated at an angular location $\pi/18$ from the cantilevered end. To assess the convergence of the proposed approach, the predictions of three expansion orders for the load distribution function were compared, $k = 0$, 2, and 4.

For loading case (a), figs. 11, 12, and 13 show the distribution of material stress components, σ_{11}, σ_{22}, and σ_{12}, respectively. The corresponding results are presented in figs. 14 to 16 for loading case (b). In these figures, the solid line shows the exact solution [38] and the predictions of the proposed approach are indicated by symbols ($\circ$), ($\diamond$), and ($\times$), for expansion orders $k = 0$, 2, and 4, respectively. For reference, the stress distributions predicted by Saint-Venant's solution ($\underline{\tau}^*_{SV}$) are shown with a dashed line.

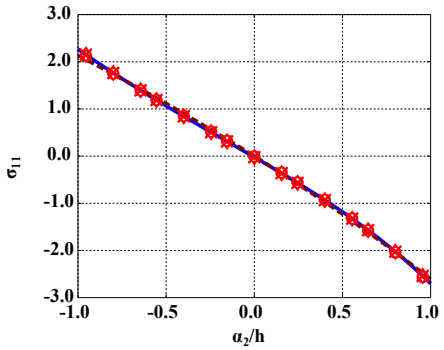

Figure 11: Distribution of stress component σ_{11}, case (a).

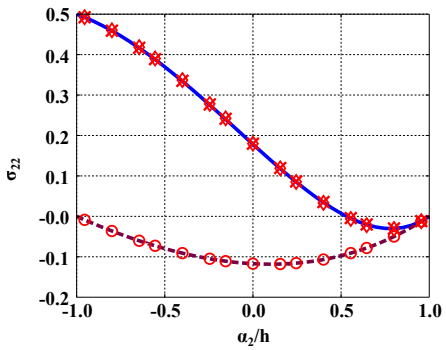

Figure 12: Distribution of stress component, σ_{22}, case (a).

In all cases, $k = 2$ gives adequate predictions, but close agreement with the exact solution requires $k = 4$ for the transverse stress component, see fig. 15. Clearly the proposed approach presents good convergence characteristics.

As observed earlier, distributed loads have little influence on axial stress distributions, see figs. 11 and 14, for loading case (a) and (b), respectively. In contrast, the effects of the distributed loading and of its spatial derivatives must be taken into account to obtain accurate predictions for shear and transverse stress components, see figs. 12 and 15.

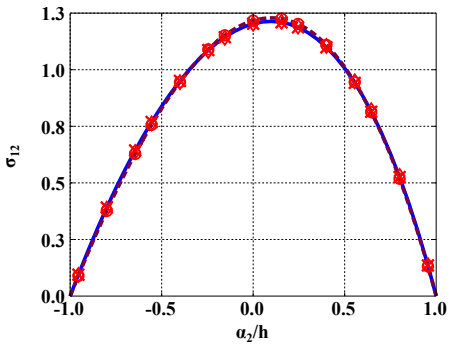

Figure 13: Distribution of the stress component, σ_{12}, case (a).

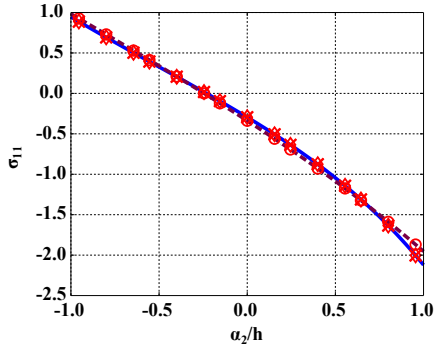

Figure 14: Distribution of the stress component, σ_{11}, case (b).

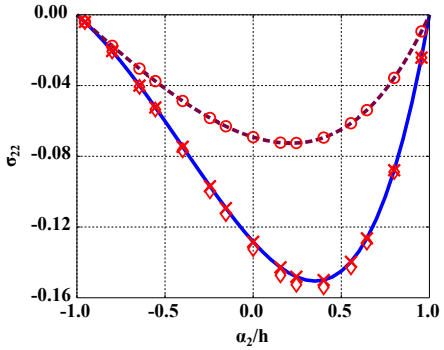

Figure 15: Distribution of the stress component, σ_{22}, case(b).

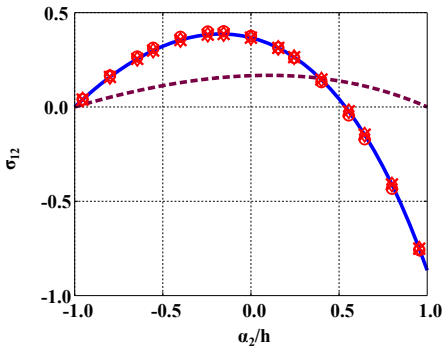

Figure 16: Distribution of the stress component, σ_{12}, case (b).

6.3 Helicoidal beam subjected to body force

The three-dimensional helicoidal beam shown in fig. 17 has a rectangular cross-section of size $b \times h$ and its reference line, which passes through the cross-section's lower-outer corner, is a helix of equation $x_1 = \rho\cos\theta$, $x_2 = \rho\sin\theta$, $x_3 = p\theta$, where $\rho = 0.35$ m is the radius and $p = 0.1$ m/rad the pitch. The beam is cantilevered at one end ($\theta = 0$) and free at the other end ($\theta = 2\pi$). Unit vectors $\bar{b}_1$, $\bar{b}_2$, and $\bar{b}_3$ are the unit tangent, normal, and binormal vectors, respectively, of the helicoidal reference line. The rotation tensor that brings basis $\mathcal{I}$ to $\mathcal{B}^*$ is denoted $\underline{\underline{R}}$ and the constant curvature vector of the beam is $\underline{k}^* = (p\bar{b}_1 + \rho\bar{b}_3)/\sigma^2$, where $\sigma^2 = p^2 + \rho^2$.

The beam is made of an isotropic material with Young's modulus $E = 73$ GPa and Poisson's ratio $\nu = 0.3$. It is subjected to constant body forces $\underline{b} = q_b\bar{\imath}_3$ and surface tractions $\underline{p} = q_t\bar{\imath}_3$ acting over the cross-section's top face, where $q_b = 1$ Nm^{-2} and q_t = -0.058 Nm^{-3}. When resolved in basis $\mathcal{B}^*$, these loading components remain constants $\underline{b}^* = \underline{\underline{R}}^T\underline{b} = q_b(p\bar{b}_1 + \rho\bar{b}_3)/\sigma$ and $\underline{p}^* = \underline{\underline{R}}^T\underline{p} = q_t(p\bar{b}_1 + \rho\bar{b}_3)/\sigma$; clearly, the distribution function is $f = 1$.

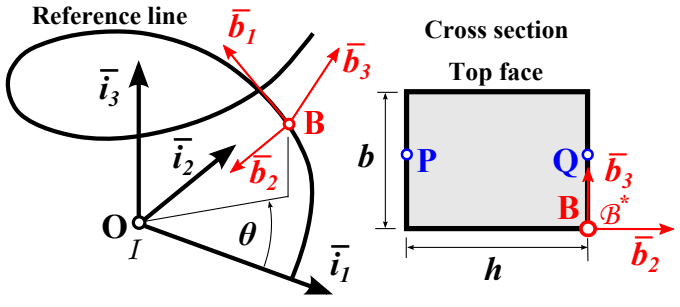

Figure 17: Configuration of the helicoidal beam

In the present approach, a two-dimensional mesh of 12×7 8-node quadrilateral elements was used to discretize the cross-section. Because the loading is uniform along the span, a zeroth order expansion ($k = 0$) of the distribution function was used. To validate the predictions, a three-dimensional FEM analysis was performed

using ABAQUS with a mesh of 12×7×302 20-node brick elements. The stress distribution over the cross-section at $\theta = 4\pi/3$ were evaluated for both approaches.

Figures 18 and 19 show the distributions of stress component σ_{22} over the cross-section predicted by ABAQUS and the present approach, respectively. For reference, the corresponding distribution predicted by Saint-Venant's solution ($\underline{\mathcal{I}}^*_{SV}$) appears in fig. 20. The corresponding results for stress component σ_{33} are shown in figs. 21 to 23. Because the body forces and surface tractions act along unit vector $\bar{b}_3$ primarily, they affect the distribution of stress component σ_{33} most significantly, as shown in fig. 23.

The stress components were also evaluated along the span of the beam at two points, **P** and **Q**, located at the mid-point of the side edges of the cross-section, as shown in fig. 17. Figures 24 and 25 show the distribution of stress components σ_{11} and σ_{33}, respectively. In these figures, the present predictions are depicted with solid lines while the symbol × indicates the ABAQUS predictions; for reference, the dotted line show Saint-Venant's solution. The present predictions are in excellent agreement with the three-dimensional FEM results, except near the beam's ends. Indeed, the present solution predicts the central solution only, and hence, cannot capture the solution near the beam's ends, which is dominated by the extremity solutions. Note that the zone affected by the extremity solutions is very small compared to the beam's span, validating the fourth assumption stated in section 5.4.

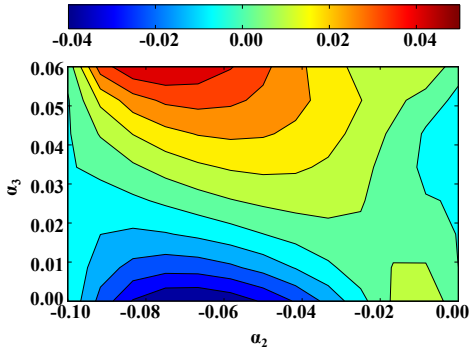

Figure 18: Distribution of stress component σ_{22}, ABAQUS.

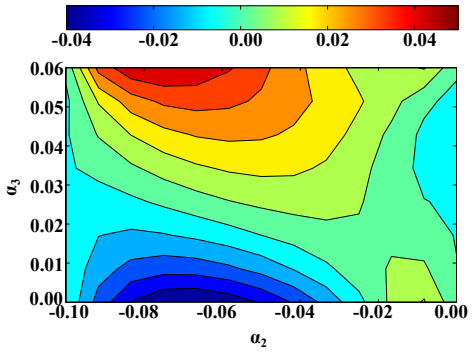

Figure 19: Distribution of stress component σ_{22}, present approach.

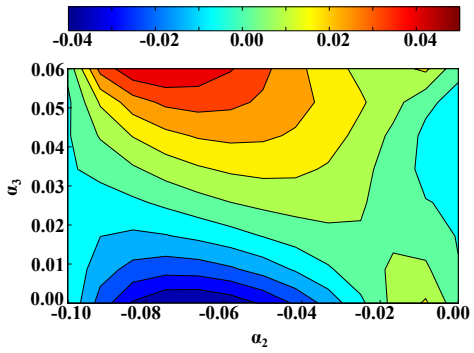

Figure 20: Distribution of stress component σ_{22}, Saint-Venant's solution.

To assess the efficiency of the proposed approach, its computational cost will be contrasted with that of the three-dimensional FEM analysis. In both cases, the main cost is the factorization of the stiffness matrix, which can be estimated [39] as $\mathcal{C} \propto nm^2$, where n is the size of the stiffness matrix and m its average half-bandwidth. For the meshes used in the three-dimensional FEM analysis and the proposed two-dimensional approach, these numbers are $n_{3D} \approx 10^5$, $m_{3D} \approx 750$ and $n_{2D} \approx 800$, $m_{2D} \approx 60$, respectively. It then follows that $\mathcal{C}_{3D}/\mathcal{C}_{2D} \approx 20,000$. For this example, the

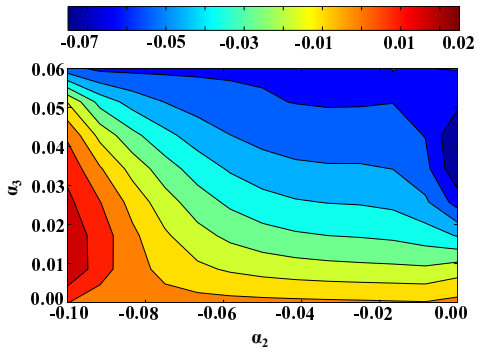

Figure 21: Distribution of stress component σ_{33}, ABAQUS.

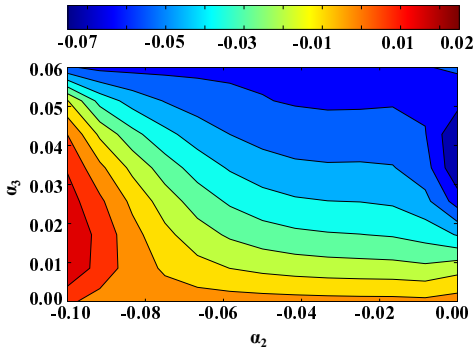

Figure 22: Distribution of stress component σ_{33}, present approach.

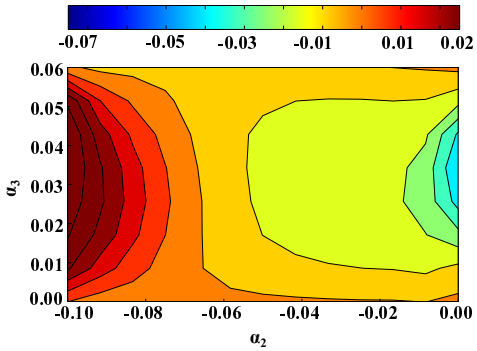

Figure 23: Distribution of stress component σ_{33}, Saint-Venant's solution.

proposed approach is four orders of magnitude more efficient than three-dimensional FEM analysis, as expected because it uses a two-dimensional discretization only.

6.4 Three-dimensional composite beam

The last example deals with the beam of length $L = 2$ m shown in fig. 26. The beam is cantilevered at one end ($\alpha_1 = 0$) and free at the other end ($\alpha_1 = L$). The cross-section is a hollow square of dimension $b = 0.1$ m consisting of two plies of graphite/epoxy material, each of thickness $t_p = 0.01$ m. The stiffness properties of the material are: longitudinal modulus $E_L = 181$ GPa, transverse modulus $E_T = 10.3$ GPa, shearing modulus $G_{LT} = 7.17$ GPa, and Poisson's ratios $\nu_{LT} = 0.28$ and $\nu_{TN} = 0.33$. The stacking sequence of two-ply lay-up is $[30°, -30°]$, as indicated in fig. 26; 0° fibers are aligned with the axis of the beam and a positive ply angle indicates a right-hand rotation about

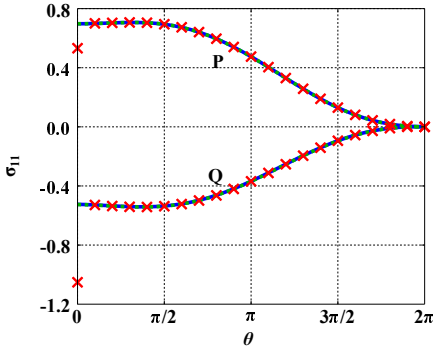

Figure 24: Distribution of stress component σ_{11} along the beam's span.

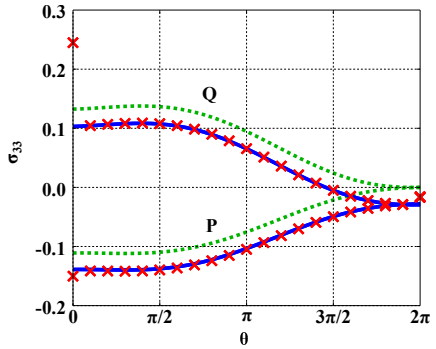

Figure 25: Distribution of stress component σ_{33} along the beam's span.

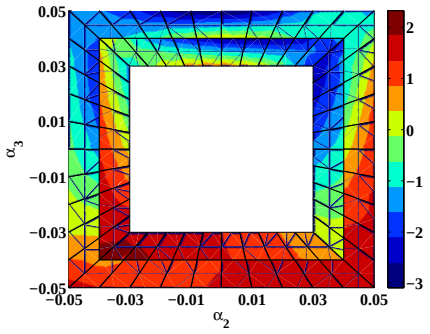

Figure 27: Distribution of the stress component σ_{11}, ABAQUS.

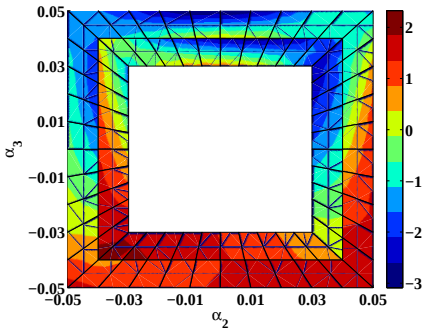

Figure 28: Distribution of the stress component σ_{11}, proposed approach.

the local outer normal to the wall. The beam is subject to surface tractions over the top face, $\underline{p} = (1 - \alpha_1/L)^2 \sin(3\pi\alpha_1/L) \cos(\pi\alpha_2/b)\bar{\imath}_3$.

The proposed approach used a mesh of 40×2, 8-node two-dimensional elements and a first-order expansion of the distribution function ($k = 1$). The predictions were compared against those of a three-dimensional FEM using a 40×2×200 mesh of 20-node brick elements in ABAQUS. Figures 27 and 28 show the distribution of stress component σ_{11} over the beam's cross-section using ABAQUS and the proposed approach, respectively. For reference, the solution of Saint-Venant's problem is shown in fig. 29. The correspond results for stress component σ_{12} are given in figs. 30 to 32.

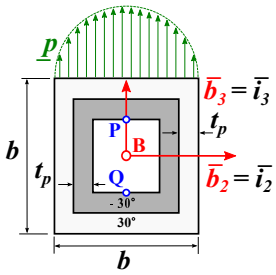

Figure 26: Configuration of the composite box cross-section.

The stress components were also evaluated along the span of the beam at two points, **P** and **Q**, located at the mid-point of the top and bottom inner edges of the cross-section, as shown in fig. 26. Figures 33 and 34 show the distribution of stress components σ_{11} and σ_{12}, respectively. In these figures, the present predictions are depicted with solid lines while the symbol × indicates the ABAQUS predictions; for reference, the dotted line show Saint-Venant's solution. In figure 34, Saint-Venant's solutions at points **P** and **Q** coincide.

Here again, the predictions of the proposed approach are in excellent agreement with those of the three-dimensional FEM analysis. Due to the presence of heterogeneous, anisotropic materials and the resulting elastic coupling, the distributed loads affect all stress components significantly. Accurate predictions are obtained only when taking into account the effects of distributed loading.

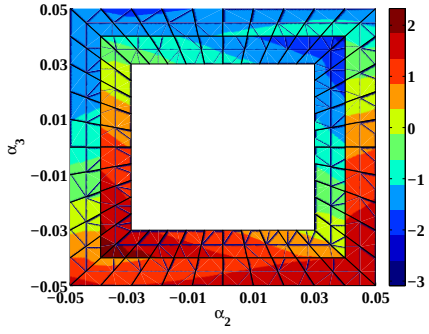

Figure 29: Distribution of the stress component σ_{11}, Saint-Venant's solution.

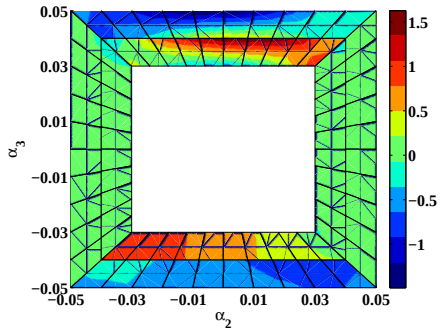

Figure 30: Distribution of the stress component σ_{12}, ABAQUS.

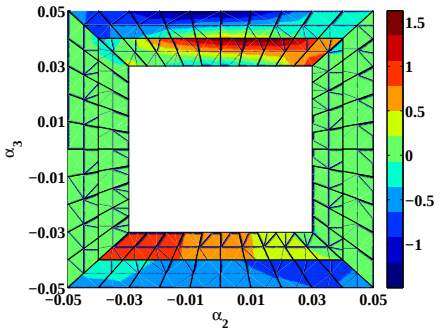

Figure 31: Distribution of the stress component σ_{12}, proposed approach.

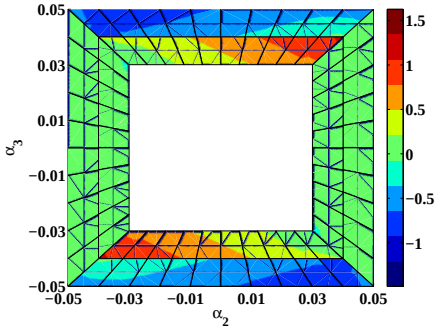

Figure 32: Distribution of the stress component σ_{12}, Saint-Venant's solution.

7 Conclusions

This paper has presented a novel approach to the solution of Almansi-Michell's problem based on Hamilton's formalism. A projection is used to reduce the three-dimensional problem to a set of ordinary differential equations. The projection is composed of two parts: a symplectic part that reduces the homogeneous problem and an additional part that takes into account the effect of the externally applied loading. Moreover, the three-dimensional strain and stress fields can be recovered from the one-dimensional solution.

Numerical examples have been presented that demonstrate the accuracy of the proposed approach by comparing its predictions with those of exact solutions of two-dimensional elasticity and of three-dimensional FEM analysis. Excellent correlation was observed in all cases. The examples also demonstrate that the effects of distributed loads must be taken into account to obtain accurate

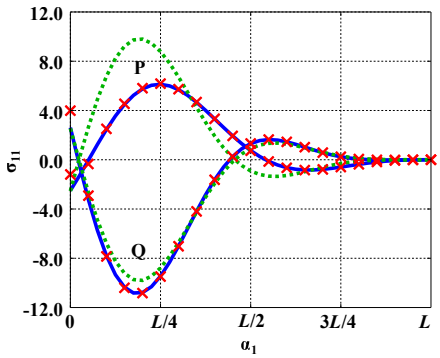

Figure 33: Distribution of the stress component σ_{11}, along the span.

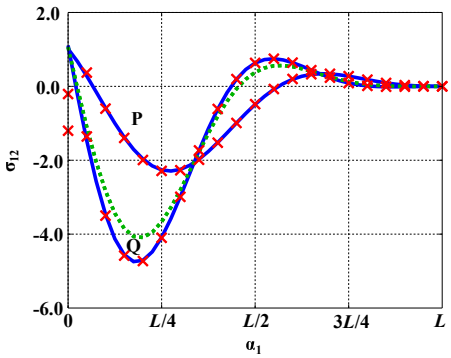

Figure 34: Distribution of the stress component σ_{12}, along the span.

stress and strain field predictions, particularly when dealing with beams made of heterogeneous, anisotropic composite materials. It was also shown that the proposed approach converges quickly as the order of expansion of the distribution function increases.

Because the proposed approach is based on a two-dimensional discretization only, it requires far less computation burden than approaches based on three-dimensional finite element discretization. Three to four orders of magnitude gains in computational efficiency were demonstrated. The present approach can be generalized to beam problems involving thermal, piezoelectric, and inertial effects.

A Hamiltonian matrices

Matrix $\underline{\underline{\mathcal{H}}}$, of size $2n \times 2n$, is said to be Hamiltonian if it satisfies the following property

$$(\underline{\underline{\mathcal{J}}}\,\underline{\underline{\mathcal{H}}})^T = \underline{\underline{\mathcal{J}}}\,\underline{\underline{\mathcal{H}}}, \tag{57}$$

where skew-symmetric matrix $\underline{\underline{\mathcal{J}}}$ is defined as

$$\underline{\underline{\mathcal{J}}} = \begin{bmatrix} \underline{\underline{0}}_{n\times n} & \underline{\underline{I}}_{n\times n} \\ -\underline{\underline{I}}_{n\times n} & \underline{\underline{0}}_{n\times n} \end{bmatrix}. \tag{58}$$

Note the following properties of matrix $\underline{\underline{\mathcal{J}}}$: $\underline{\underline{\mathcal{J}}}^T = -\underline{\underline{\mathcal{J}}}$, $\underline{\underline{\mathcal{J}}}\,\underline{\underline{\mathcal{J}}}^T = \underline{\underline{\mathcal{I}}}$.

Property (57) implies that the most general form of a Hamiltonian matrix is

$$\underline{\underline{\mathcal{H}}} = \begin{bmatrix} \underline{\underline{A}} & \underline{\underline{B}} \\ \underline{\underline{C}} & -\underline{\underline{A}}^T \end{bmatrix}, \tag{59}$$

where matrices $\underline{\underline{A}}$, $\underline{\underline{B}}$, and $\underline{\underline{C}}$ are of size $n \times n$ and matrices $\underline{\underline{B}}$ and $\underline{\underline{C}}$ are symmetric.

B Symplectic transformations

Two vectors, $\underline{\mathcal{X}}$ and $\underline{\mathcal{Y}}$, both of size $2n \times 1$, are said to be symplectic orthogonal if they satisfy the following property $\underline{\mathcal{X}}^T\,\underline{\underline{\mathcal{J}}}\,\underline{\mathcal{Y}} = 0$. Matrix $\underline{\underline{\mathcal{S}}}$, of size $2n \times 2m$ ($m \leq n$), is said to be symplectic if it satisfies the following property

$$\underline{\underline{\mathcal{S}}}^T\,\underline{\underline{\mathcal{J}}}\,\underline{\underline{\mathcal{S}}} = \underline{\underline{\hat{\mathcal{J}}}}, \tag{60}$$

where skew-symmetric matrix $\underline{\underline{\hat{\mathcal{J}}}}$ is of size $2m \times 2m$ but otherwise identical to that defined by eq. (58). Each column of matrix $\underline{\underline{\mathcal{S}}}$ is symplectic orthogonal to its other columns.

Consider now the following transformation

$$\underline{\underline{\mathcal{H}}}\,\underline{\underline{\mathcal{S}}} = \underline{\underline{\mathcal{S}}}\,\underline{\underline{\hat{\mathcal{H}}}}. \tag{61}$$

Pre-multiplying this equation by $\underline{\underline{\mathcal{S}}}^T\,\underline{\underline{\mathcal{J}}}$ yields $\underline{\underline{\mathcal{S}}}^T(\underline{\underline{\mathcal{J}}}\,\underline{\underline{\mathcal{H}}})\,\underline{\underline{\mathcal{S}}} = \underline{\underline{\mathcal{S}}}^T\,\underline{\underline{\mathcal{J}}}\,\underline{\underline{\mathcal{S}}}\,\underline{\underline{\hat{\mathcal{H}}}} = (\underline{\underline{\hat{\mathcal{J}}}}\,\underline{\underline{\hat{\mathcal{H}}}})$ and hence, if matrix $\underline{\underline{\mathcal{H}}}$ is Hamiltonian, so is matrix $\underline{\underline{\hat{\mathcal{H}}}}$. Clearly, transformation (61) is structure preserving: Hamiltonian matrix $\underline{\underline{\mathcal{H}}}$, of size $2n \times 2n$, is reduced to Hamiltonian matrix $\underline{\underline{\hat{\mathcal{H}}}}$, of size $2m \times 2m$, by symplectic matrix $\underline{\underline{\mathcal{S}}}$.

C Solvability condition

Considering a linear system of the following form

$$\underline{\underline{\mathcal{H}}}\,\underline{\mathcal{X}} = \underline{\mathcal{Y}}, \tag{62}$$

where matrix $\underline{\underline{\mathcal{H}}}$ is a singular Hamiltonian matrix of null space $\underline{\underline{\mathcal{N}}}$ such that $\underline{\underline{\mathcal{H}}}\,\underline{\underline{\mathcal{N}}} = \underline{\underline{0}}$. Multiplying both sides of this equation by $\underline{\underline{\mathcal{J}}}$ leads to $\underline{\underline{\mathcal{H}}}^T(\underline{\underline{\mathcal{J}}}^T\underline{\mathcal{X}}) = \underline{\underline{\mathcal{J}}}\,\underline{\mathcal{Y}}$, where property (57) was used. Solutions of this linear system exist if and only if the right-hand side vector is orthogonal to the null space of matrix $\underline{\underline{\mathcal{H}}}$,

$$\underline{\underline{\mathcal{N}}}^T\underline{\underline{\mathcal{J}}}\,\underline{\mathcal{Y}} = \underline{0}. \tag{63}$$

Linear system (62) is solvable if and only if the right-hand side, $\underline{\mathcal{Y}}$, is symplectic orthogonal with the null space of the coefficient matrix $\underline{\underline{\mathcal{H}}}$. This solvability condition is first found by Zhong [25].

References

[1] J. C.-B. de Saint-Venant. Mémoire sur la torsion des prismes. *Receuil des Savants Étrangers*, 14:233–560, 1855.

[2] J. C.-B. de Saint-Venant. Mémoire sur la flexion des prismes. *Journal de Mathématiques de Liouville*, 1:89–189, 1856.

[3] J.H. Michell. The theory of uniformly loaded beams. *The Quarterly Journal of Pure and Applied Mathematics*, 32:28–42, 1901.

[4] E. Almansi. Sopra la deformazione dei cilinri solecitati lateralmente. *Atti della Reale Accademia Nazionale dei Lincei, Classe Scienze Fisiche, Matematiche e Naturali*, 5:400–408, 1901.

[5] S.P. Timoshenko and J.N. Goodier. *Theory of Elasticity*. McGraw-Hill Book Company, New York, third edition, 1970.

[6] A.E.H. Love. *A Treatise on The Mathematical Theory of Elasticity*. Dover Publications, Inc., New York, fourth edition, 1944.

[7] O.A. Bauchau and J.I. Craig. *Structural Analysis with Application to Aerospace Structures*. Springer, Dordrecht, Heidelberg, London, New-York, 2009.

[8] D. Ieşan. Saint-Venant's problem for inhomogeneous and anisotropic elastic bodies. *Journal of Elasticity*, 6(3):277–294, 1976.

[9] D. Ieşan. On Saint-Venant's problem. *Archive for Rational Mechanics and Analysis*, 91(4):363–373, 1986.

[10] S.B. Dong, J.B. Kosmatka, and H.C. Lin. On Saint-Venant's problem for an inhomogeneous, anisotropic cylinder - Part I: Methodology for Saint-Venant solutions. *Journal of Applied Mechanics*, 68(3):376–381, 2000.

[11] H.C. Lin and S.B. Dong. On the Almansi-Michell problems for an inhomogeneous, anisotropic cylinder. *Journal of Mechanics*, 22:51–57, 2006.

[12] C.W. Liu and E. Taciroglu. A semi-analytic meshfree method for Almansi-Michell problems of piezoelectric cylinders. *International Journal of Solids and Structures*, 45(9):2379–2398, 2008.

[13] H.C. Lin, J.B. Kosmatka, and S.B. Dong. On Saint-Venant's problem for an inhomogeneous, anisotropic cylinder-Part III: End effects. *Journal of Applied Mechanics*, 68(3):392–398, 2001.

[14] H. Bai, A.H. Shah, S.B. Dong, and E. Taciroglu. End reflections in a layered piezoelectric circular cylinder. *International Journal of Solids and Structures*, 43(20):6309–6325, 2006.

[15] V.L. Berdichevsky. On the energy of an elastic rod. *Prikladnaya Matematika y Mekanika*, 45(4):518–529, 1982.

[16] A.R. Atilgan and D.H. Hodges. Unified nonlinear analysis for nonhomogeneous anisotropic beams with closed cross-sections. *AIAA Journal*, 29(11):1990–1999, November 1991.

[17] D.H. Hodges. *Nonlinear Composite Beam Theory*. AIAA, Reston, Virginia, 2006.

[18] W.B. Yu. Cross-sectional analysis of composite beams with distributed loads. In *Proceedings of the 32nd ASME Wind Energy Symposium*, National Harbor, Maryland, 13-17 January 2014.

[19] V. Giavotto, M. Borri, P. Mantegazza, G. Ghiringhelli, V. Carmaschi, G.C. Maffioli, and F. Mussi. Anisotropic beam theory and applications. *Computers & Structures*, 16(1-4):403–413, 1983.

[20] M. Borri, G.L. Ghiringhelli, and T. Merlini. Linear analysis of naturally curved and twisted anisotropic beams. *Composites Engineering*, 2(5-7):433–456, 1992.

[21] P. Masarati. On the semi-analytical solution of beams subjected to distributed loads. In *Proceedings of the XVI Congresso Nazionale AIDAA*, Palermo, Italy, 24-28 September 2001.

[22] A. Mielke. Saint-Venant's problem and semi-inverse solutions in nonlinear elasticity. *Archive of Rational Mechanics and Analysis*, 102:205–229, 1988.

[23] A. Mielke. Normal hyperbolicity of center manifolds and Saint-Venant's principle. *Archive of Rational Mechanics and Analysis*, 110:353–372, December 1990.

[24] W.X. Zhong. Plane elasticity problem in strip domain and Hamiltonian system. *Journal of Dalian University of Technology*, 4:373–384, 1991.

[25] W.X. Zhong. *A New Systematic Methodology for Theory of Elasticity*. Dalian University of Technology Press, Dalian, 1995.

[26] B.Q. Zhu, J.F. Zhou, and J.S. Zhuo. Symplectic solution of rectangular beam subjected to distributed load. *Mechanics in Engineering*, 29(3):15–19, 2007.

[27] P. Ladevèze and J. Simmonds. New concepts for linear beam theory with arbitrary geometry and loading. *European Journal of Mechanics - A/Solids*, 17(3):377–402, 1998.

[28] R. El Fatmi and H. Zenzri. On the structural behavior and the Saint-Venant solution in the exact beam theory: Application to laminated composite beams. *Computers & Structures*, 80(16-17):1441–1456, 2002.

[29] R. El Fatmi and H. Zenzri. A numerical method for the exact elastic beam theory. Applications to homogeneous and composite beams. *International Journal of Solids and Structures*, 41(9-10):2521–2537, 2004.

[30] O. Rand and V. Rovenski. *Analytical Methods in Anisotropic Elasticity with Symbolic Computational Tools*. Springer, Birkhäuser, 2007.

[31] J.R. Barber. Three-dimensional elasticity problems for the prismatic bar. *Proceedings of the Royal Society of London A: Mathematical, Physical and Engineering Sciences*, 462(2070):1877–1896, 2006.

[32] O.A. Bauchau and S.L. Han. Three-dimensional beam theory for flexible multibody dynamics. *Journal of Computational and Nonlinear Dynamics*, 9(4):041011 (12 pages), 2014.

[33] S.L. Han and O.A. Bauchau. Nonlinear three-dimensional beam theory for flexible multibody dynamics. *Multibody System Dynamics*, 34(3):211–242, July 2015.

[34] O.A. Bauchau. *Flexible Multibody Dynamics*. Springer, Dordrecht, Heidelberg, London, New-York, 2011.

[35] C. Lanczos. *The Variational Principles of Mechanics*. Dover Publications, Inc., New York, 1970.

[36] C. Alpdogan, S.B. Dong, and E. Taciroglu. A method of analysis for end and transitional effects in anisotropic cylinders. *International Journal of Solids and Structures*, 47(7-8):947–956, 2010.

[37] T. Kailath. *Linear Systems*. Prentice-Hall, Englewood Cliffs, NJ, 1980.

[38] H.J. Ding, N.L. Peng, and Y. Li. The curved bar subjected to an arbitrary distributed loading – another paradox in the two-dimensional theory of elasticity. *Acta Mechanica Solida Sinica*, 17(4):360–364, December 1996.

[39] K.J. Bathe. *Finite Element Procedures*. Prentice Hall, Inc., Englewood Cliffs, New Jersey, 1996.